Energy Research and Development Division

FINAL PROJECT REPORT

Minichannel Technology to Improve Solar Water Heaters

California Energy Commission

Gavin Newsom, Governor

January 2019 | CEC-500-2019-008

PREPARED BY:

Primary Author(s):
Gerardo Diaz, Principal Investigator
Van Duong, Graduate Student Researcher

University of California, Merced
5200 North Lake Road
Merced, CA 95343
Phone: 209-228-7858| Fax: 209-228-4047
http://faculty.ucmerced.edu/gdiaz

Contract Number: 500-10-048

PREPARED FOR:
California Energy Commission

Jeffrey Doll
Project Manager

Virginia Lew
Office Manager
ENERGY EFFICIENCY RESEARCH OFFICE

Laurie ten Hope
Deputy Director
ENERGY RESEARCH AND DEVELOPMENT DIVISION

Drew Bohan
Executive Director

ACKNOWLEDGEMENTS

The author would like to thank Ed Silva, Justin McConnell and Bryan Spielman for fabricating the aluminum and copper minichannel collectors, and Kevin Rico and Kevin Balkoski for their help with the system installation. In addition, the author would also like to thank the undergraduate students who worked and contributed to this research project: Azucena Robles, Adam Martin, Jose Guadarrama, and Keith Saechao.

PREFACE

The California Energy Commission Energy Research and Development Division supports public interest energy research and development that will help improve the quality of life in California by bringing environmentally safe, affordable, and reliable energy services and products to the marketplace.

The Energy Research and Development Division conducts public interest research, development, and demonstration (RD&D) projects to benefit California.

The Energy Research and Development Division strives to conduct the most promising public interest energy research by partnering with RD&D entities, including individuals, businesses, utilities, and public or private research institutions.

Energy Research and Development Division funding efforts are focused on the following RD&D program areas:

- Buildings End-Use Energy Efficiency
- Energy Innovations Small Grants
- Energy-Related Environmental Research
- Energy Systems Integration
- Environmentally Preferred Advanced Generation
- Industrial/Agricultural/Water End-Use Energy Efficiency
- Renewable Energy Technologies
- Transportation

Minichannel Technology to Improve Solar Water Heaters is the final report for the Minichannel Technology to Improve Solar Water Heaters project (contract number 500-10-048, or UC-CIEE award number POEF01-M04) conducted by Gerardo Diaz Research Group at the University of California, Merced. The information from this project contributes to the Energy Research and Development Division's Energy Systems Integration Program.

For more information about the Energy Research and Development Division, please visit the Energy Commission's website at www.energy.ca.gov/research/ or contact the Energy Commission at 916-327-1551.

ABSTRACT

Water heaters are the second highest source of energy consumption in residential households in the United States. While most common systems use natural gas or electricity to heat water, solar water heaters are receiving more attention because of its lower operating costs. Common solar water heater designs include flat-plate collectors and evacuated tubes with a heat-pipe attached to an absorber fin. Generally, copper is used for fabricating these collectors because of its favorable heat transfer properties. However, other thermal designs use different materials, such as aluminum, without loss of performance. These thermal design systems include minichannel technology. Minichannel technology is found in the automotive, electronics cooling and HVAC industries due to its excellent thermal performance.

This final report describes the design and manufacturing of an aluminum minichannel tube solar water heater. Experimental design and market outlook of the aluminum minichannel solar water heater is described as well. Year-long test results and performance are presented with comparison to an identically sized copper flat-plate solar collector. A computational model is developed and shared to present a computational tool to predict the aluminum minichannel solar water heater performance.

The researchers also examined the potential use of copper minichannel technology for medium temperature application and steam generation including its design, manufacturing and experimental design.

Keywords: minichannel, solar collector, solar water heater, aluminum, copper

Please use the following citation for this report:

Diaz, Gerardo. (University of California-Merced). 2015. *Minichannel Technology to Improve Solar Water Heaters.* California Energy Commission. Publication number: CEC-500-2019-008.

TABLE OF CONTENTS

LIST OF FIGURES

LIST OF TABLES

EXECUTIVE SUMMARY

Introduction

Residential and commercial water heating consumes a significant amount of energy. In California, water heating is the most significant residential end use for natural gas. Ninety percent of homes in the state use natural gas to heat water, which represents 49 percent of the average annual household natural gas consumption. More than 11 million households use natural gas water heaters, with 2,111 million therms of natural gas consumed each year. There are different types of water heating options in the market, with the most common systems using electricity or natural gas.

Solar energy, including solar thermal, has been of interest for decades. With large operating ranges and various solar collector configurations, solar thermal has been used in many different applications and industries, including the food processing industry, residential and commercial water heating, and water desalination technology. Ongoing improvements in efficiency have shown that solar thermal applications have been increasingly adopted.

Since the first patented solar water heater there have been numerous collector designs, with flat-plate collectors and evacuated tube solar collectors being widely used in the residential market. Compound parabolic solar concentrators are also widely used for solar thermal power generation but have limited industrial applications for solar water heating. Research on solar water heaters continues to focus on the efficiency of transferring the energy from the sun to the working fluid that runs through the collectors to heat the water. Increasing the efficiency can reduce the use of natural gas and other fuels in residential and commercial sectors.

In the residential market, the two most popular solar water heaters are the flat-plate and evacuated tube solar collectors. In a flat-plate design, multiple round-pipes are equally spaced and attached to a thin plate of copper (the absorber plate) by ultrasonic welding. However, only a small section of the round pipe's circumference is in contact with the absorber through the weld. The second design, the evacuated tube solar collector, consists of a copper pipe (the heat pipe) welded to a copper fin (the absorber fin) placed inside a vacuum glass tube to reduce heat loss. Some of the main issues with this design are the relative small size of the condenser section, which limits the rate of heat transfer to the heat pipe, keeping the internal glass tube in a vacuum. Both designs have optimization and efficiency limitations.

Minichannel solar collectors are proposed as an alternative to improve heat transfer in a solar hot water collector. A few companies such as Chengyi and Savo Solar currently manufacture flat minichannel solar water heaters. However, long-term performance and design analysis of minichannel solar water heaters are not currently available.

Project Purpose and Process

This project analyzed the design and performance of minichannel solar water heaters, found in the automotive and HVAC industries (but novel to solar thermal applications) that coupled a more efficient heat exchanger design with lower cost aluminum minichannels. The first phase of this project compared the performance of an aluminum minichannel solar water heater with

a conventional copper flat-plate solar water heater built to residential and commercial standards.

The overall demonstration test setup of the aluminum-based minichannel solar water heater includes the collector, pump, piping, water storage tank and sensors. A control logic programmed with LabView using National Instruments data acquisition system to control the system and collect test results and data. Researchers measured and collected data on the inlet and outlet temperatures of the working fluid, temperature of the water storage tank that exchanged heat energy with the working fluid, flow rate of the working fluid, and solar irradiance.

Based on the success of the project's first phase, the second phase would test the performance of a copper minichannel solar water heater. Copper is favored for its material and heat transfer properties. Researchers explored the design and manufacturing of the copper minichannel solar water heater and were able to achieve preliminary results on their performance from initial testing.

Project Results

The team tested (1) an aluminum based minichannel solar water heater, and (2) a copper minichannel solar collector for the purpose of generating low-grade steam.

Experimental results from testing an aluminum minichannel solar water heater show an increase in efficiency when compared to a conventional copper, flat-plate solar water heater. The minichannel design does not require a flat fin to be attached to the tube to transfer heat to the working fluid, as do traditional flat-plate solar water heaters. The team compared the performance of the aluminum solar collector to that of a flat-plate solar collector, using the same external components and operating conditions. The results were an increase of 13 percent in thermal absorption compared to a conventional flat-plate collector.

To better understand the operation of the aluminum minichannel, project researchers developed and validated a mathematical model of the aluminum collector using test data from the project. Even though aluminum does not conduct heat as well as copper, the aluminum system was able to heat the water just as well as a conventional copper collector.

Results of preliminary testing of the minichannel collector show potential to generate steam until late afternoon, extending the system's production capabilities. This is because the collector is able to stay above 100 degrees Celsius (212 degrees Fahrenheit) late into the day.

Project Benefits

The aluminum minichannel solar water heater has the potential to reduce costs and increase efficiency of solar collectors on the market. Aluminum is less expensive than copper, the material used in conventional solar water heaters. And it provides an alternative configuration to currently available technologies for solar water heating. Aluminum minichannels are also more efficient at low temperatures (less than 100 degrees Celsius) than conventional copper flat-plate collectors.

The researchers also examined the potential use of copper minichannel technology for medium temperature application and steam generation including its design, manufacturing and experimental design. The copper minichannel solar water heater requires more research, however, it has the potential to provide a cost effective solution to generating medium temperatures with the potential of generating steam for appropriate applications (such as industrial low pressure steam processes).

Creating a solar water heating configuration with reduced costs and increased efficiency, has the potential to increase the use of solar thermal in California. The average cost for a California residential solar water system in 2011 was $8,364.32. Approximately 30 percent of this cost are for the collectors. If the price of collectors can be substantially reduced, widespread installation of cleaner solar energy systems can be achieved, decreasing the dependence on natural gas for water heating in California.

CHAPTER 1:
Design, Computational Model and Manufacture of Aluminum Minichannel Solar Water Heaters

Water heating accounts for a significant amount of energy consumption in California - nearly half of natural gas consumption in the residential sector and nearly a third of natural gas consumption in the commercial sector.[1] For instance, residential water heating is often the second largest energy use in a house and, in many cases, it accounts for nearly a quarter of overall household energy consumption.[2] Standard electric storage tank systems have been found to have the highest energy cost compared to other technologies (Newport Partners, 2011). Other technologies translate into lower operating costs but require the use of natural gas, propane, or other fuels.

Solar thermal systems provide the capability of generating low to medium grade heat in a sustainable way and for a variety of applications due to the relatively large range of temperatures that different collector configurations provide. A key issue that remains a subject of intense research is how to effectively transfer the energy obtained from the sun to the working fluid in a solar thermal system. Increasing the efficiency in solar thermal systems such as solar water heaters has the potential to have a high impact on the consumption of natural gas and other fuels in the residential and commercial sector.

Design and Manufacturing

Currently, the price of copper[3] is more than three times the price of aluminum[4] so there is an incentive to develop a solar application that uses aluminum instead of copper. The thermal conductivity of copper is about 1.8 times the conductivity of aluminum so the thermal design needs to account for this disparity.

Most solar water heater designs currently being sold in the market include using a plate or fin attached to a pipe, which carries the working fluid (Figure 1). To reduce cost, the plate thickness tends to only be a fraction of a millimeter so that the heat absorbed by the collector can be transferred through this thin plate. The plate is bonded to the pipe on a few locations, usually by means of ultrasonic welding.

---

[1] Natural Gas Energy Efficiency in Buildings: Roadmap for Future Research, p. 14, http://www.energy.ca.gov/2014publications/CEC-500-2014-036/CEC-500-2014-036-F.pdf .

[2] Natural Gas Energy Efficiency in Buildings: Roadmap for Future Research, Figures 5 and 6, http://www.energy.ca.gov/2014publications/CEC-500-2014-036/CEC-500-2014-036-F.pdf.

[3] http://www.infomine.com/investment/metal-prices/copper/.

[4] http://www.infomine.com/investment/metal-prices/aluminum/.

Figure 1: Ultrasonic Welding of Solar Collectors

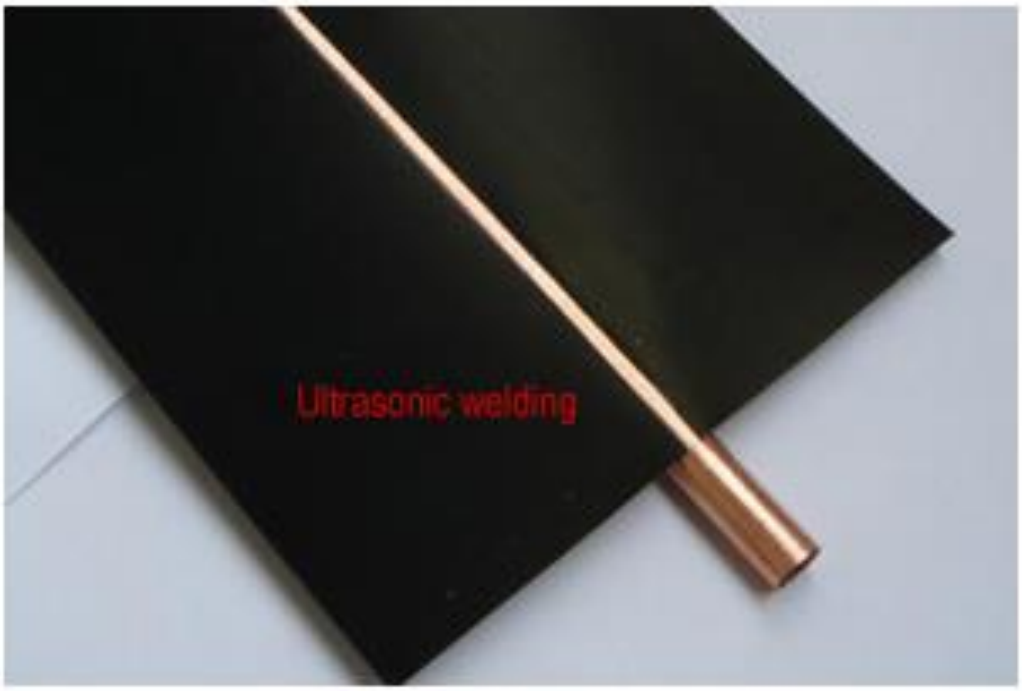

Source: www.toponesolar.com

A design was conceived (Diaz, 2008; Sharma et al., 2011a; Sharma et al., 2011b; Diaz, 2013) so that the solar energy directly reaches the tube carrying the working fluid, rather than being transferred through a fin or thin plate. The selective coating typically applied to a conventional flat-plate collector is applied directly on the tube instead of on the surface of the plate (Figure 2).

Figure 2: Comparing Conventional Flat Plate Design and Minichannel Solar Water Heater

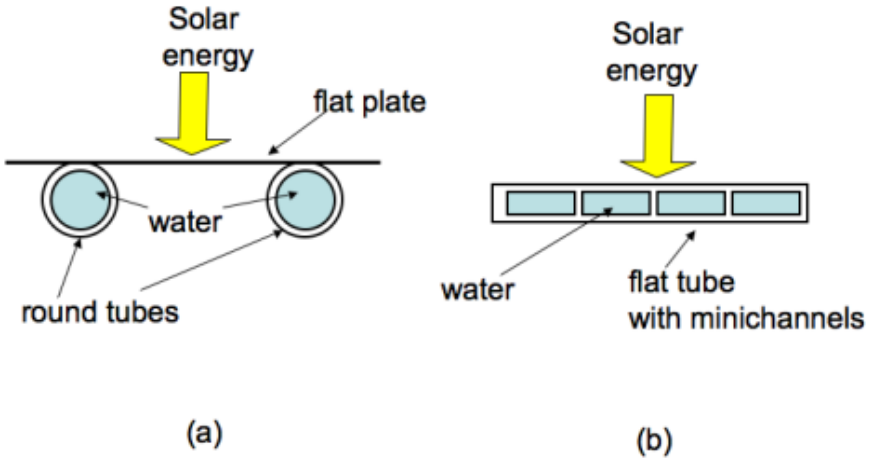

a: flat-plate design; b: minichannel design

Source: University of California, Merced

A multi-port extrusion (MPE) aluminum tube was obtained from the company Hydro Aluminum[5] to be used in manufacturing the solar collector. The MPE aluminum tube was obtained from the company [6] with a design featuring a width of 100 mm and a height of 2 mm with minichannels on the cross sectional area of the tube (Figure 3).

Figure 3: Aluminum Minichannel Tube

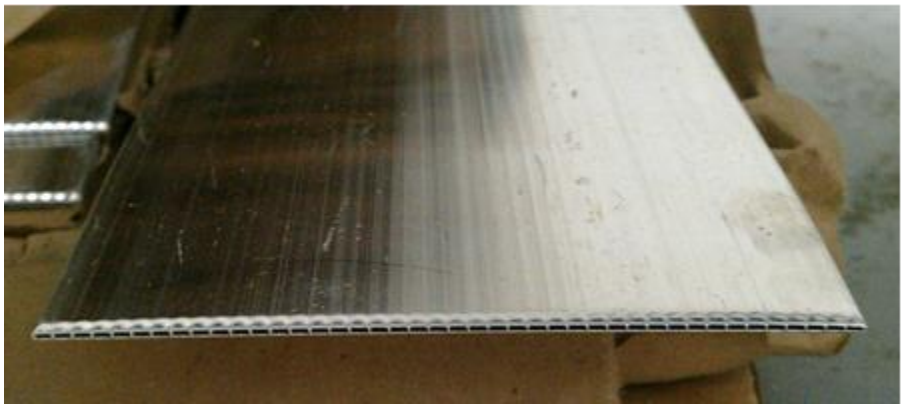

Source: University of California, Merced

Tubes were ordered at 2.94 meters long to fit into a standard solar water heater frame currently available in the market. Frames were obtained from the company SunEarth, which have a gross area of 3.8 square meters and utilize a low-iron tempered glass. Side insulation of Polysocyanurate and a back insulation material composed of Polysocyanurate and Fiberglass were used. Black Chrome (EC Series) with a minimum absorptivity of 95 percent and a maximum emissivity of 12 percent was sprayed on the surface of the tubes.

The design of the aluminum collector included an inlet and an outlet header with the minichannel tubes inserted in between. Figure 4 shows the design of the collector before the selective coating was sprayed.

The water heater configuration utilized eleven tubes in parallel with a separation of 9 mm between tubes. Vacuum brazing technology is typically utilized in the automotive and air conditioning industries to bond the tubes to the header. However, due to the dimensions of the solar water heater, there were no vacuum brazing ovens found in the vicinity of the project that fit the researcher's needs. Therefore, the bonding of the tubes to the header was completed using tungsten inert gas (TIG) welding. The separation of the tubes was necessary to allow the nozzle of the TIG welding unit to reach the side of the tubes (Figure 5). If it were possible to use vacuum brazing, then this separation can be reduced.

[5] http://www.hydro.com/.

Figure 4: Design of Aluminum Minichannel Solar Water Heater

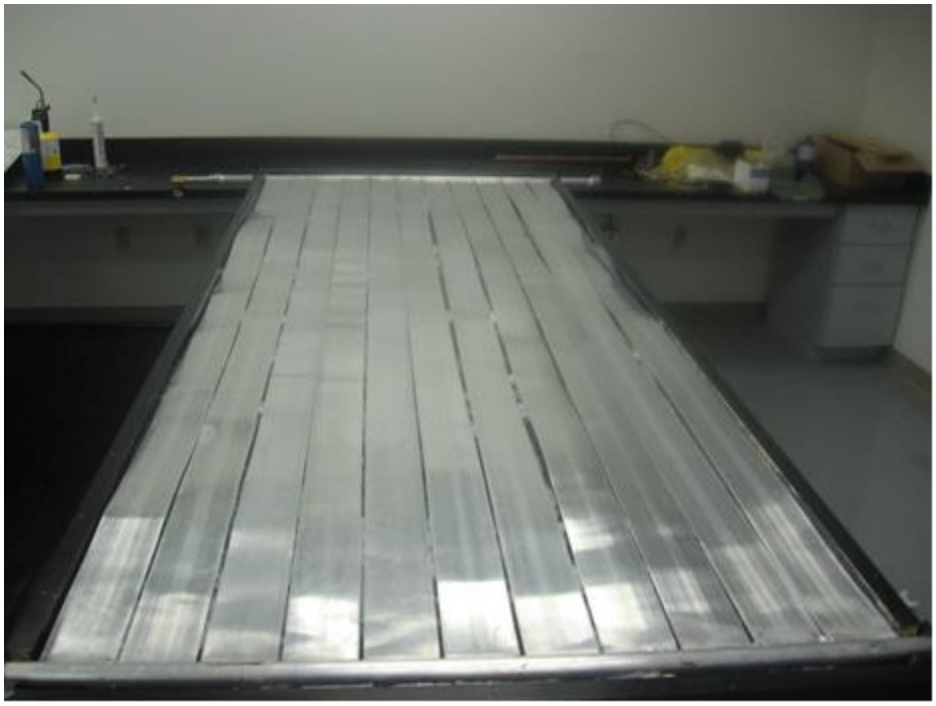

Selective coating was sprayed on the surface of the aluminum tubes.

Source: University of California, Merced

Figure 5: TIG Welding of the Aluminum Solar Water Heater

UC Merced facilities personnel performs TIG welding

Source: University of California, Merced

The selective coating was sprayed on the top surface of the aluminum tubes (Figure 6). The final product is the aluminum collector which is placed inside a standard collector frame with the low-iron tempered glass placed on top (Figure 7).

Figure 6: Applying Selective Coating to the Surface of the Aluminum Minichannel Solar Water Heater

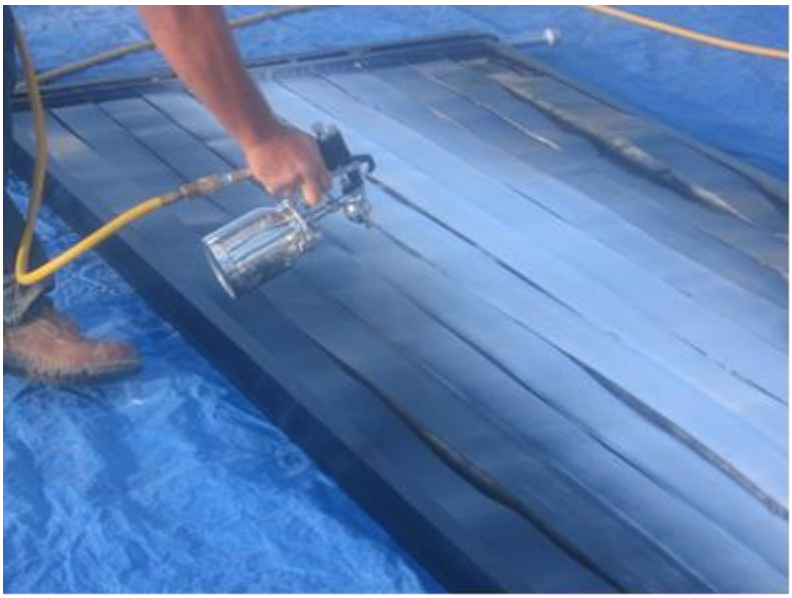

Source: University of California, Merced

Figure 7: Final Assembly of the Aluminum-based Minichannel Solar Water Heater

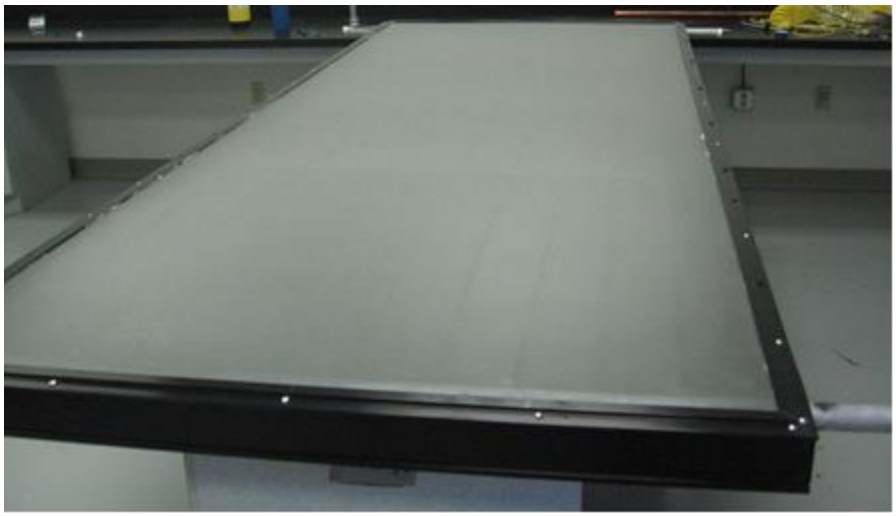

Source: University of California, Merced

For performance comparison, a standard copper plate-and-tube solar water heater was also constructed with the same dimensions of the aluminum core (2.9 m x 1.2 m, approximately). More detailed difference in dimensions of the aluminum minichannel and copper flat-plate solar collector are shown in Table 1. High temperature solder was used to bond the plate to the tubes and the same Black Chrome (EC Series) selective coating was sprayed on top of the plate surface.

Table 1: Comparison of Aluminum Minichannel and Copper Flat-plate Solar Collectors Dimensions

	Aluminum Minichannel	Copper Flat-Plate
Dimensions of Collector		
Frame length	3048 mm	3048 mm
Frame width	1219 mm	1219 mm
Absorber area	3.20 m^2	3.61 m^2
Total free flow area	1015.5 mm^2	712.2 mm^2
Dimensions of Tube		
Hydraulic diameter of each tube	1.42 mm	9.53 mm
Width (major)	100 mm	—
Height (minor)	2 mm	—
Length	2912 mm	2912 mm
Number of tubes	11	10

Source: University of California, Merced

Figure 8 shows the final copper collector configuration.

Figure 8: Final Assembly of the Copper Flat-plate Solar Water Heater

Source: University of California, Merced

Both collectors were installed next to each other at the University of California, Merced's Castle facilities. A closed-loop configuration with a 50/50 mixture of propylene glycol and water was

used to transfer the energy obtained at the solar collector to water inside an 80-gallon (300-liter) storage tank. Each system operates independently from each other and each collector feeds a single storage tank. Table 1 shows the difference in dimensions of the aluminum minichannel and copper flat-plate solar collector.

Computational Model

The performance of the aluminum based solar water heater is also being studied computationally by developing a simulation tool that predicts the heat transfer, thermal efficiency, pressure drop, and outlet temperatures of the collector based on inlet temperature, solar irradiance, volumetric flow rate, ambient temperature, and ambient air velocity. The code was developed utilizing the commercial software Engineering Equation Solver (EES, 2014). Energy and mass balances were performed at the glass cover, absorber/glass cover gap, absorber and tube sections. These energy balances are described below and the variables described in Table 2.

Energy Balance Equations for Glass Cover

The variables used in the governing equations are defined in Table 2. Appendix D provides examples of how these equations were derived and how the model was developed.

Equation 1:

$$q''_{in} + q''_{rad\_Ag} + q''_{conv\_gair} = q''_{conv\_gsky} + q''_{rad\_gsky} + q''_{absorbed}$$

Equation 1a:

$$G_s + \left[h_{rad_{Ag}}\sigma\left(T_{Abs}^4 - T_g^4\right)\right] + \left[h_{air}\left(T_{air} - T_g\right)\right] = \left[h_o\left(T_g - T_\infty\right)\right] + \left[h_{rad_{gsky}}\sigma\left(T_g^4 - T_{sky}^4\right)\right] + \left[Absorb_{coeff}G_s\right]$$

Equation 1b:

$$G_s + \left[\left(\frac{1}{\frac{1}{\varepsilon_g} + \frac{1}{\varepsilon_{Abs}} - 1}\right)\sigma\left(T_{Abs}^4 - T_g^4\right)\right] + \left[h_{air}\left(T_{air} - T_g\right)\right] = \left[h_o\left(T_g - T_\infty\right)\right] + \left[\left(\varepsilon_g\right)\sigma\left(T_g^4 - T_{sky}^4\right)\right] + \left[\left(\frac{\alpha_{Abs}\tau_g}{\left(1 - (1 - \alpha_{Abs})\rho_g\right)}\right)G_s\right]$$

Energy Balance Equations for the Section of Air between the Glass and Absorber

Equation 2:

$$q''_{conv\_Aair} = q''_{conv\_gair}$$

Equation 2a:

$$h_{air}\left(T_{Abs} - T_{air}\right) = h_{air}\left(T_{air} - T_g\right)$$

Energy Balance Equations for the Absorber

Equation 3:

$$q''_{absorbed} = q''_{conv\_Aair} + q''_{rad\_Ag} + q''_{cond}$$

Equation 3a:

$$\left(\frac{\alpha_{Abs}\tau_g}{(1-(1-\alpha_{Abs})\rho_g)}\right)G_s = [h_{air}(T_{Abs} - T_{air})] + \left[h_{rad_{Ag}}\sigma(T_{Abs}^4 - T_g^4)\right] + \left[\frac{\frac{T_{Abs} - T_{fluid}}{R_{total}}}{L_{tube} * major}\right]$$

Equation 3b:

$$R_{total} = R_{Abs} + R_{Al} + R_{fluid}$$

Equation 3c:

$$R_{total} = \left[\frac{AbsorbThick}{k_{Abs}(L_{tube} * major)}\right] + \left[\frac{TubeWalls}{k_{Al}(L_{tube} * major)}\right] + [N_{ports}(\eta_o h_{fluid} A_t)^{-1}]$$

Validation

Validation of the mathematical model against the experimental results of the aluminum minichannel solar collector is presented in Chapter 2, Test Results.

Table 2: Descriptions of Variables

Variable	Units	Description
α_{Abs}	none	Absorption Coefficient of Absorber
A_t	m^2	Total Surface Area of One Tube (Array)
$Absorb_{coeff}$	none	Absorption Coefficient
$AbsorbThick$	m	Thickness of the Absorber Selective Coating
ε_g	none	Emissivity of glass
ε_{Abs}	none	Emissivity of absorber
G_s	W/m^2	Total Incident Radiation
h_{air}	W/m^2-K	Convection heat transfer coefficient of air between glass and absorber
h_{fluid}	W/m^2-K	Heat transfer coefficient of the fluid through convection
h_o	W/m^2-K	Convection coefficient of glass/ambient air
h_{rad_Ag}	W/m^2-K	Radiation heat transfer coefficient between the absorber and glass
$h_{rad_{gsky}}$	W/m^2-K	Radiation heat transfer coefficient between the glass and sky
k_{Abs}	W/m-K	Thermal conductivity of the absorber
k_{Al}	W/m-K	Thermal conductivity of aluminum
L_{tube}	m	Length of the tube (array)

Variable	Units	Description
$major$	m	Width of the tube (array)
η_o	none	Overall efficiency of tube (array)
N_{ports}	none	Number of ports in array
ρ_g	none	Reflectivity of the glass
$q"_{absorbed}$	W/m^2	Net absorption by the selective coating of the transmitted solar irradiance
$q"_{cond}$	W/m^2	Heat transferred by conduction from the absorber to the working fluid
$q"_{conv\_Aair}$	W/m^2	Heat loss by air convection on the inner surface of the glass
$q"_{conv\_gair}$	W/m^2	Heat loss by air convection on the inner surface of the glass
$q"_{conv_{gsky}}$	W/m^2	Heat loss by air convection on the outer surface of the glass
$q"_{in}$	W/m^2	Heat absorption by the glass in the solar spectrum
$q"_{rad\_Ag}$	W/m^2	Net heat transfer from the absorber to the glass
$q"_{rad\_gsky}$	W/m^2	Net heat transfer from the glass to the sky (atmosphere)
R_{Abs}	K/W	Thermal Resistance of Absorber through Conduction
R_{Al}	K/W	Thermal Resistance through Conduction in Aluminum
R_{fluid}	K/W	Thermal Resistance through Convection to the Fluid
R_{total}	K/W	Total thermal resistance between absorber and working fluid
σ	W/m^2-K^4	Stefan-Boltzmann constant
T_{Abs}	K	Temperature at the Absorber
T_{air}	K	Temperature of the Air between Glass and Absorber
T_{fluid}	K	Temperature of the fluid
T_g	K	Temperature at the Glass
τ_g	none	Transmissivity of the glass
T_{sky}	K	Temperature of the sky
T_∞	K	Ambient temperature
$TubeWalls$	m	Thickness of the tube walls

Source: University of California, Merced

CHAPTER 2:
Test Plans and Test Results for the Aluminum-based Minichannel Solar Water Heater

In California, water heating in the residential and commercial sectors accounts for a significant amount of energy consumption. In households, water heating is often the second largest source of energy consumption. In addition, water heating accounts for nearly a quarter of overall energy use in households. The highest energy costs are found in standard electric water storage tank systems compared to other technologies (Newport Partners, 2011). Other technologies may have lower operating costs but require the use of fuels such as natural gas or propane.

Solar thermal technology is capable of providing low to medium heat temperature in a sustainable way. Because of its capability of providing a large range of temperatures, there are various applications for solar thermal technology such as water heating, pool heating, or space heating. The issue that remains in any renewable energy technology is always efficiency. For solar thermal water heating, the issue is effectively transferring heat energy from the sun to the working fluid. Increasing the efficiency of solar water heating can lead to a potential reduction in the usage of natural gas and other fuels for water heating in the residential and commercial sectors. Moreover, if a lower cost material can be selected that leverages a more efficient design, then this can improve the efficiency and cost effectiveness of solar thermal technology.

This demonstration used a minichannel design found in the automotive and heating, ventilation, and air conditioning (HVAC) industries (but novel to solar thermal applications) that coupled a more efficient heat transfer design with lower cost aluminum minichannels. The overall demonstration setup of the aluminum-based minichannel solar water heater includes the collector, pump, piping, water storage tank and sensors. A control logic programmed with LabView using National Instruments CompactDAQ[6] as a data acquisition system was utilized to control the system and collect test results and data. Researchers measured and collected data on the inlet and outlet temperatures of the working fluid, temperature of the water storage tank that exchanged heat energy with the working fluid, flow rate of the working fluid, and solar irradiance.

To compare the performance of the aluminum-based minichannel solar water heater, a conventional copper flat-plate solar water heater with identical dimensions and system components was built and installed alongside the aluminum-based system. Both solar water heater systems were installed beside each other at the Castle facilities at the University of

[6] CompactDAQ is a portable digital acquisition (DAQ) platform that integrates connectivity and signal conditioning into modular input/output for directly interfacing to any sensor or signal typically used for vehicle data logging and benchtop research projects.

California, Merced, and they were in operation for more than a year, collecting data on daily and per minute intervals, from February 2013 to May 2014.

Experimental Set-Up

The aluminum-based minichannel solar water heater system has the following main components: collector, pump, water storage tank, and control logic as shown in Figure 9.

Figure 9: Diagram of Experimental Set-up of the Solar Water Heater

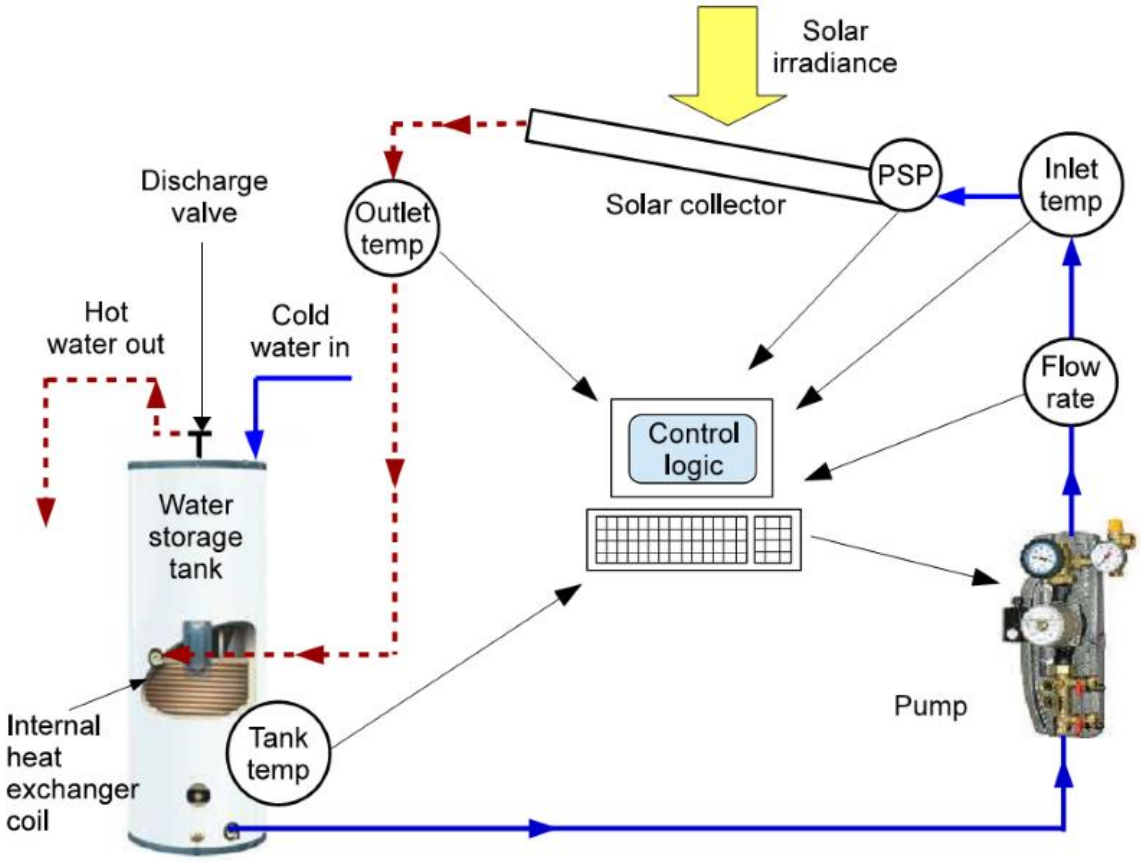

Source: University of California, Merced

The solar water heater system had sensors such as thermocouples to measure inlet and outlet temperature of the working fluid entering and exiting the collector, and to measure the tank water temperature that the working fluid exchanged heat energy with; a volumetric flow meter to measure the flow rate of the working fluid circulating the system; a precision spectral pyranometer to measure the solar irradiance, or the amount of solar energy hitting the collectors.

The system was remotely operated by control logic programmed using LabView. When the program detects a solar irradiance measurement of 150 W/m^2 or greater, the pump turns on circulating the working fluid through the closed-loop system. The working fluid used was a 50-50 percent mixture of propylene glycol and water. As the pump circulates the working fluid through the water storage tank, the working fluid exchanges heat energy with the water by

means of an internal heat exchanger. At the instance when the control logic detects the water storage tank at a safety limit of 55 ˚C or greater, the discharge valve of the storage tank is opened to release the hot water and replenishes the tank with cooler water until the temperature of the tank falls to 30 ˚C. Temperatures, flow rate and solar irradiance data were measured by the sensors and collected daily at a per minute basis.

The copper flat-plate solar water heater also had an identical set-up and system operation. Both solar water heater systems were built, installed and operated the same way as any conventional solar water heater systems would on any residential household. The only difference is the number of collectors installed.

Test Plan

The objective of the aluminum-based minichannel solar water heater was to test and observe whether it can operate as a standard solar water heater for residential and commercial purposes. One way to test this objective was to evaluate the performance of the aluminum minichannel solar water heater in comparison to the copper flat-plate solar water heater. A copper flat-plate solar water heater was built and installed alongside the aluminum-based minichannel solar water heater.

At sunrise before the aluminum-based minichannel and copper flat-plate solar water heater systems are turned on, the tank temperatures for both systems are checked to make sure they are at similar temperatures. This way the researchers can make an adequate comparison of the daily performances knowing that the water storage tanks for the aluminum-based minichannel and copper flat-plate solar water collectors started at the same temperature at the start of the day. If not, the water in the storage tank with a higher temperature will be drained and refilled with cooler water. Once the tank temperatures are checked and calibrated, both solar water heater systems are turned on for the day. The systems will operate throughout the day as described above. The systems are turned off after sunsets and remain off during the night.

The system was monitored and measurements were logged daily using the data acquisition system. Measurements, such as the water temperature in the storage tank, inlet and outlet temperatures of the working fluid in the collectors, solar irradiance, and flow rate of the working fluid were logged. The data was collected minute by minute and logged daily for over a year from February 2013 to May 2014. The data measured was used in an analysis to assess the daily performance of the collector. The test plans include a performance comparison of the aluminum-based minichannel and the copper flat-plate solar water heaters on different days and seasons of the year.

In addition, comparisons were made of the daily weather conditions to observe the severity of degradation in performance of the collectors on cloudy or rainy days. Other test plans include optimizing the system and increasing the efficiency by testing the systems at different operating flow rates. With the pump installed, an option of low, medium or high speed flow rate can be selected. Changing the speed of the flow rate can result in changes in pressure drop in the collectors. Overall, it can affect the performance and efficiency of the system.

Test Results

The following plots, taken from (Robles et al., 2014), show some data analysis the researchers performed on the minichannel solar water heater. Figure 10 shows the performance of the aluminum minichannel solar water heater on two different days: (a) spring day, April 12, 2013, and (b) summer day, June 21, 2013. The plots outline the water storage tank, the ambient, and the glycol-water fluid inlet and outlet temperatures, along with the solar irradiance throughout the day. From the solar irradiation measured on the spring day (Figure 10, [a]), based on the data, it can be inferred that the weather conditions were overcast in the afternoon, which directly affected the working fluid inlet and outlet temperatures.

On the warmer summer day (Figure 10, [b]), it can be inferred from the plot that the weather conditions were sunny throughout the day. The water storage tank temperature reached 55 ˚C between 4:45 pm and 6:45 pm, which trigged the discharge valve to open and release the hot water and adding cooler water to the tank. When the water storage tank temperature fell to 30 ˚C, the discharge valve closed and the system continued to heat the water.

Figure 10: Aluminum Minichannel Solar Water Heater Performance on a Spring and Summer Day

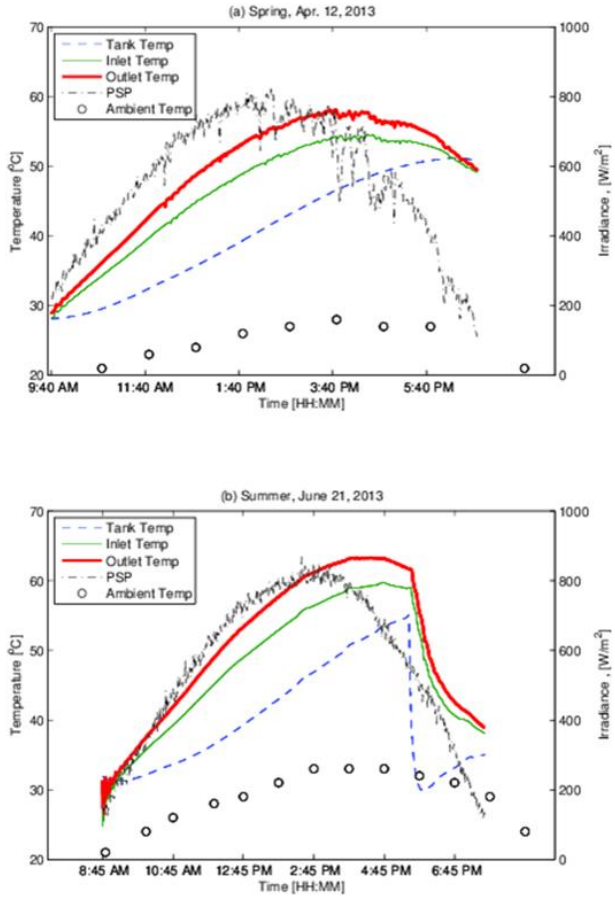

(a) **Spring day (April 12, 2013), and (b) Summer day (June 21, 2013)**

Source: University of California, Merced

To show the performance of the aluminum minichannel solar water heater within the year that it was tested, Figure 11 compares both the aluminum minichannel and the copper flat-plate system on a randomly picked day in each season of the year.

Figure 11: Seasonal Comparison of the Aluminum Minichannel and Copper Flat-plate Solar Water Heater Storage Tank

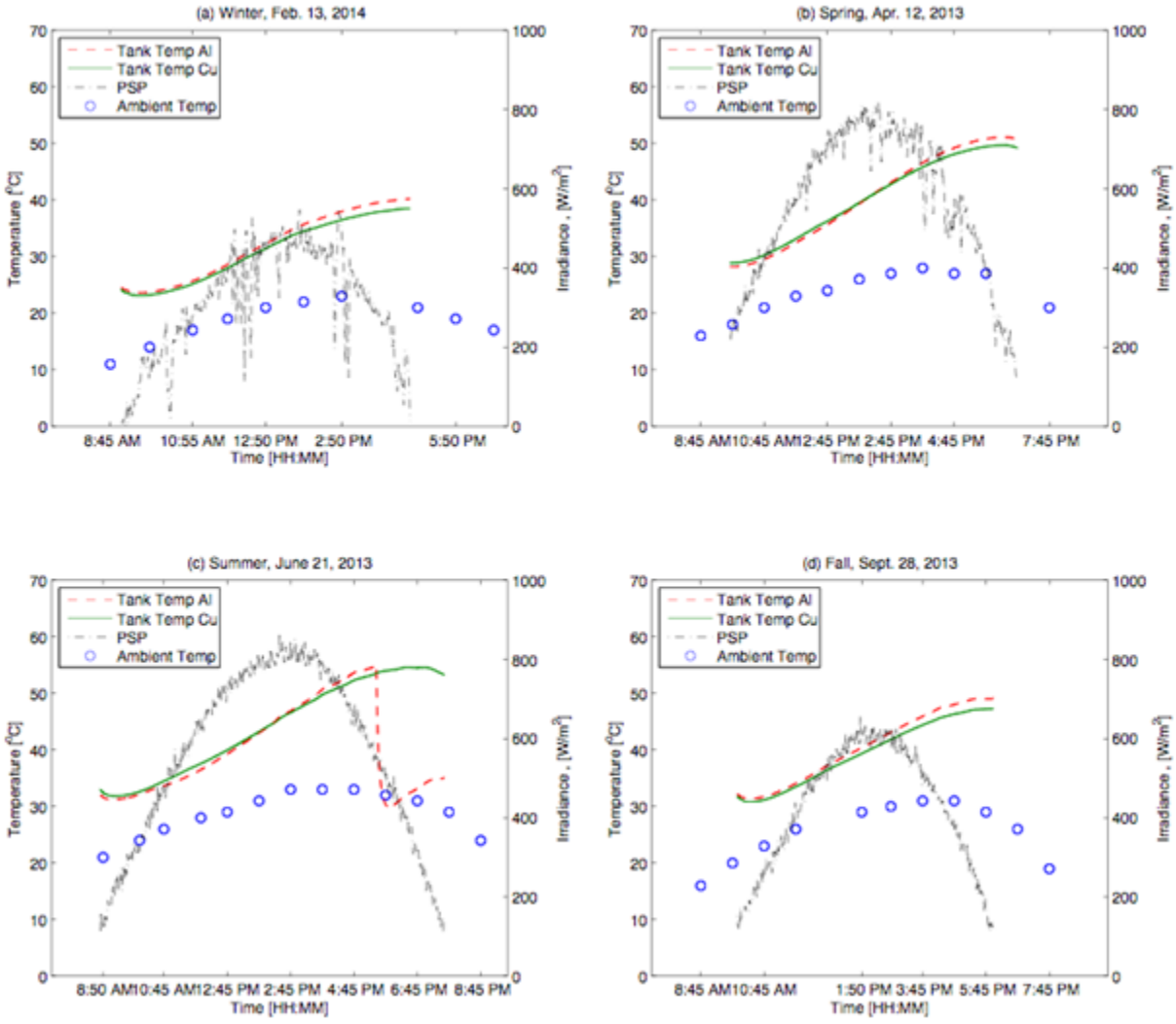

(a) Winter (February 13, 2014), (b) Spring (April 13, 2013), (c) Summer (June 21, 2013), (d) Fall (September 28, 2013).

Source: University of California, Merced

The randomly selected day in Figure 11(a) shows oscillations of the solar irradiance line, implying that the weather conditions on this day were cloudy. The temperatures were 52.5 degrees F in the morning and 62.8 degrees F in the afternoon. However, despite the cold weather, the water storage tank temperature of the aluminum minichannel steadily increased throughout the day from 24.6 degrees C and peaking at 40.2 degrees C. From Figure 11(b), the water storage tank temperature of the copper flat-plate started a little higher than the aluminum minichannel with a tank inlet temperature of 29.7 degrees C. By the afternoon, the

water storage tank temperature of the aluminum minichannel collector slowly surpassed the copper flat-plate collector, and ended up a degree or two higher than the copper flat-plate collector by the end of the day. Figure 11(c) shows a summer day and is a good example of the water storage tank temperature in the aluminum minichannel solar water heater reaching 55 degrees C to trigger the discharge valve to open. The tank temperature in the copper flat-plate was not able to reach 55 degrees C that day. On a fall day, Figure 11(d) shows the same pattern as in winter and spring, where the temperature of the water storage tank of the aluminum minichannel system achieved a higher peak temperature than the copper flat-plate system.

Another method used to assess the performance of the aluminum minichannel collector was to compare the thermal efficiency of both solar water heaters. A spring day, April 24, 2013, was chosen and the thermal efficiency was plotted against time of day as seen in Figure 12. It can be clearly seen that the efficiency of the aluminum minichannel was about 10-15 percent higher than the flat-plate collector.

Figure 12: Efficiency Comparison of the Experimental Aluminum Minichannel and Copper Flat-plate Solar Water Heater

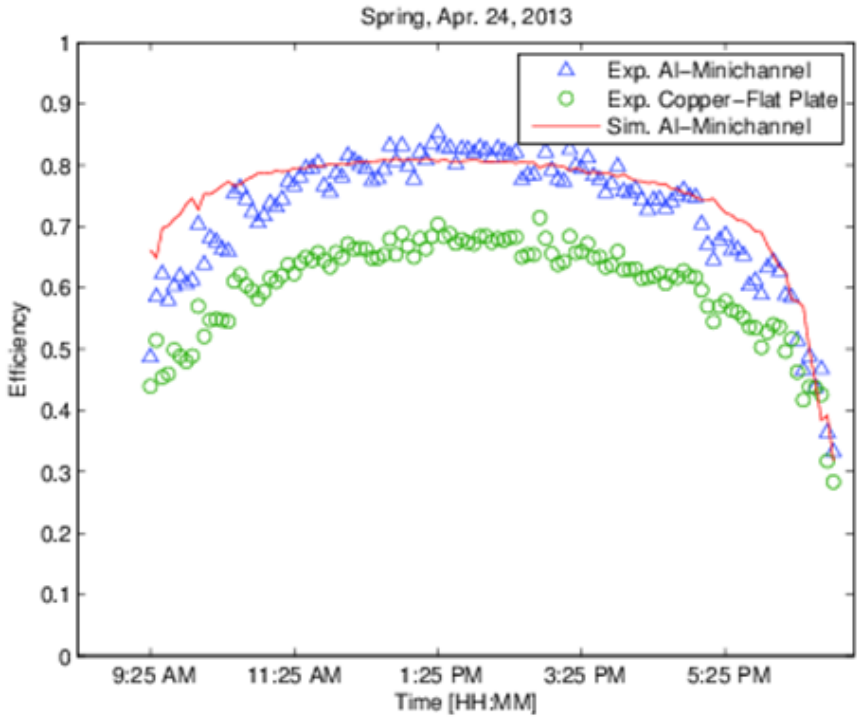

A simulation model of the aluminum minichannel is also shown.

Source: University of California, Merced

To run additional tests where operating conditions can be manipulated, the researchers developed a mathematical model of the aluminum minichannel solar water heater. Figure 12 shows the simulation of the mathematical model, in addition to the thermal efficiency plot, using the same operating conditions as the experiment during that day. This means that the inlet working fluid temperature, ambient temperature, wind speed, solar irradiance, and

volumetric flow rate of the working fluid data taken from the experiment or external sources, such as an online archive of weather history for the ambient temperature (Weather Underground, 2014), were used as operating conditions to run the simulation of the mathematical model. The results show that the mathematical model gives a reasonable approximation of the experimental data. A discrepancy in the mathematical model is that it assumes steady-state conditions. In the beginning of the plot (or morning), it can be seen that the simulation model overestimates the temperature. This overestimation is because thermal inertia was not considered in the simulation methodology. However, as the simulation progresses through the day, the simulation improves and provides a better approximation of the thermal efficiency.

Figure 13 shows another efficiency plot of the same day, however, instead of plotting efficiency against time of day, efficiency is plotted against $(T_{inlet} - T_{ambient})/G$, a standard parameter used for efficiency plots in solar thermal energy.

Figure 13: Efficiency Comparison of Experimental Data of the Aluminum Minichannel and Copper Flat-plate and Simulated Mathematical Model of the Aluminum Minichannel

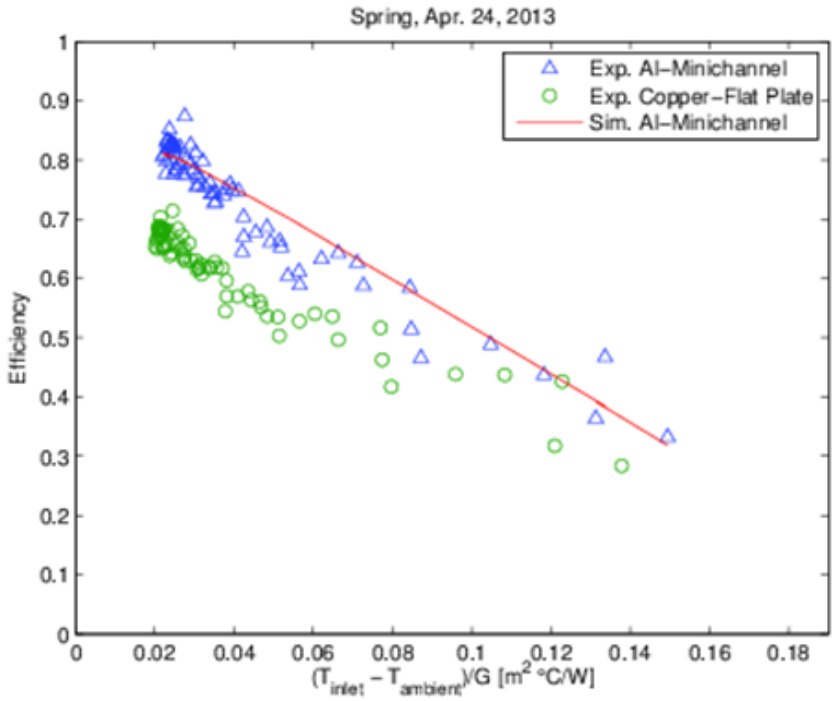

Source: University of California, Merced

In this plot, T_{inlet} is the inlet temperature of the working fluid, $T_{ambient}$ is the ambient temperature and G is the solar irradiance. Again, it can be seen that the efficiency of the experimental aluminum minichannel solar water heater system is higher than the copper flat-plate solar water heater system. The mathematical model simulation of the aluminum minichannel solar water heater shows reasonable agreement with the experimental data.

CHAPTER 3:
Market Size, Changes in Design, and Manufacturing Process

In the United States, the energy consumption of the residential and commercial sectors accounts for 40 percent of the country's total primary energy consumption (Hudson et al., 2012). Within the total household energy consumption, 20 percent accounts for water heating (Cassard et al., 2011). Water heating technology comes in different forms depending on the energy source utilized. Therefore costs such as installation, maintenance and operations can vary significantly. According to a recent technical report, water heating systems that use electric heating in water storage tanks have been found to have the highest energy and operating costs compared to other technologies (Newport Partners, 2011). Other types of systems can have lower energy and operating costs, but require using fuels such as natural gas or propane.

Solar thermal water heating systems have been around since the late 19th century. The earliest solar water heating collector invented was in 1891, when C. M. Kemp patented an "apparatus for utilizing the sun's rays" to heat up water (Kemp, 1891). Solar water heaters have grown in popularity during the past decades with copper flat-plate and evacuated tubes being the most popular solar thermal designs. Solar thermal systems have shown the capability of providing low to medium temperature heat in a sustainable way, and common applications include pool, space and water heating. One of the areas of active research in solar thermal systems concerns the effective transfer of heat from the sun to a working fluid. High impact in energy consumption can be obtained by increasing the efficiency of solar collectors. The project team has made great strides in this field of research.

Since February 2012, a prototype of an aluminum-based minichannel solar water heater was designed, built and installed at the Castle facilities of University of California, Merced. A conventional copper flat-plate collector with similar dimensions was also built to compare the performance of the aluminum minichannel solar water heater. Data was collected on a daily basis and analyzed to assess the performance of the two collectors. Due to the effective heat transfer design of the aluminum minichannel tubes, the aluminum minichannel solar water heater system has outperformed the traditional copper flat-plate solar water heater (Robles et al., 2014).

The performance of the minichannel tubes shows that there is potential for marketability and interest in this type of technology. However, before commercialization can be considered, it is necessary to study the market size potential. If the market size and interest is promising, changes in design are necessary to optimize the technology and manufacturing process for mass production.

Market Size

Solar technology has been gaining awareness and popularity throughout the years. According to the Solar Energy Industries Association (SEIA), solar water heating installation capacity has been steadily growing. As seen in Figure 14, 2.4 million square feet of collectors were sold in 2010 (SEIA, 2013); an increase of 5 percent of installation capacity from the previous year.

Figure 14: Steady Growth of Solar Water Heating Capacity Installations by Year in the United States

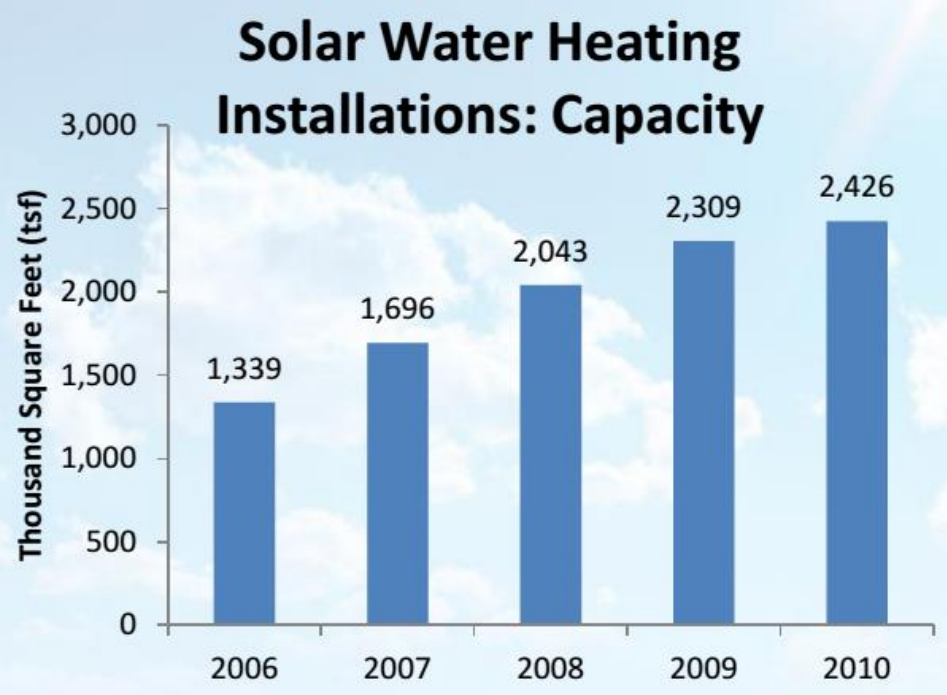

Source: Solar Energy Industries Association 2013, United States Solar Market Insight Report.

In addition, some states are promoting and trying to encourage solar water heating systems or other solar thermal technologies in the residential and commercial sectors by offering rebates and other incentives. These states are Arizona, California, Hawaii, North Carolina, Massachusetts, Pennsylvania, Florida and Oregon (CPUC, 2014; Murray, 2010). Other states offer savings, tax credit and loan programs when purchasing and installing a solar water heater system in the residential or commercial sectors. More information about rebates, tax credit and savings in a particular state can be searched on the Federal Government's Energy web portal (Energy.gov, 2014; Proske, 2010).

The aluminum-based minichannel solar water heater has the potential to replace the flat-plate solar water heater and its associated market. In terms of market size, it will depend on how private companies and the state governments promote and market solar thermal water heater systems in the residential and commercial sector with tax credits, rebates and other incentives. In Table 3, according to the United States Solar Market Insight Report: 2011 Solar Heating and Cooling Year-In-Review, the market in 2011 has shown that 40,389 square feet of solar water

heating (SWH) collectors were installed in the residential sector and 97,283 square feet of SWH collectors were installed in the non-residential sector, giving California a total of 138,122 square feet of SWH collector installed in 2011 (GTM Research and SEIA, 2011).. These numbers were collected primarily from incentive program administrators, and utility companies, manufacturers and installers that chose to participate.

Table 3: Solar Water Heating Systems Installed Capacity (square feet) in 2011

	Residential	Non-Residential	Total
AZ	135,607	14,620	150,227
CA	40,839	97,283	138,122
CT	5,374	-	5,374
DC	-	25,000	25,000
DE	269	128	397
HI	138,533	-	138,533
IL	1,157	845	2,002
MA	10,905	16,628	27,533
MD	15,596	160	15,756
ME	16,559	-	16,559
MN	2,460	1,901	4,361
NC	3,114	126,195	129,309
NH	14,032	2,498	16,529
NY	7,600	-	7,600
OR	4,099	9,450	13,549
PA	15,359	10,080	25,439
TX	3,075	360	3,435
VT	17,378	10,990	28,368
WI	16,976	-	16,976
Total	448,930	316,138	635,760

Source: GTM Research and SEIA, 2011

Lack of awareness of the technology and the lack of potential state and federal incentives, tax credits and savings have delayed the growth of solar water heater system installations. More importantly, in states such as California that predominantly use natural gas for water heating, the decreasing price of natural gas has affected the growth of solar water heater installations. In 2007, California Assembly Bill 1470 assumed that the price of natural gas would increase from 2010 to 2017. However, due to the economic crisis of October 2008 and the introduction of new drilling techniques, prices of natural gas ($/Mcf) have fallen since 2008, as seen in Figure 15 and Figure 16, in the United States and California, respectively (CPUC, 2014). Due to reduction of natural gas prices, the growth of solar water heating installations has been slow.

Figure 15: Annual Natural Gas Prices in the United States

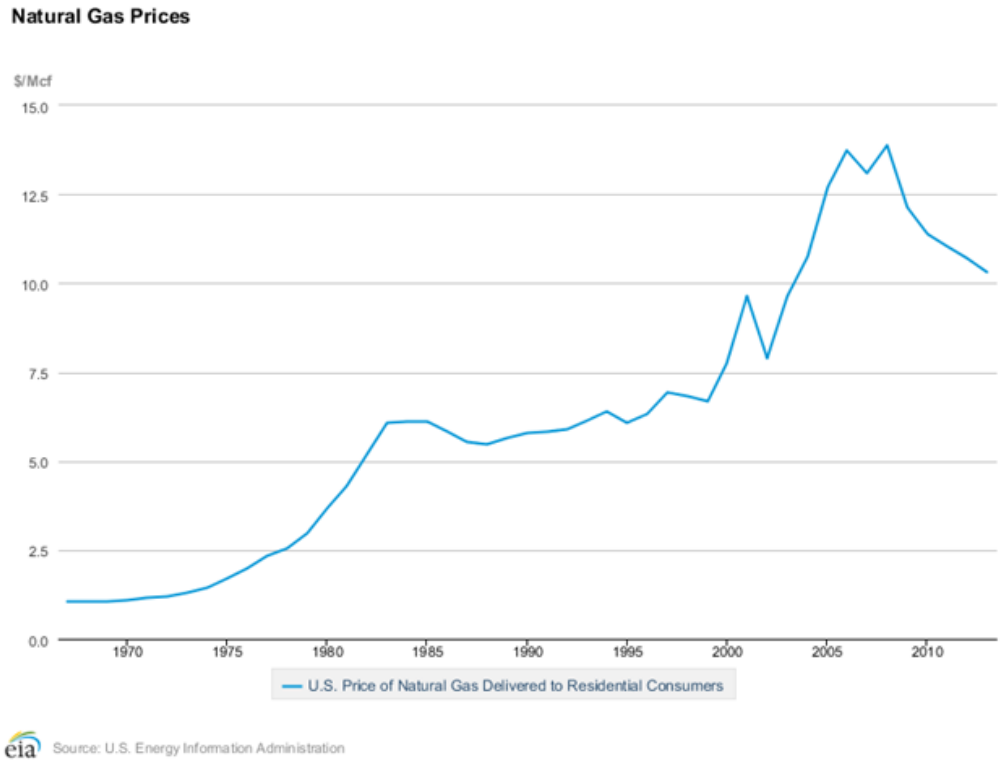

Source: United States Energy Information Administration (2014)

Figure 16: Annual Natural Gas Prices in California

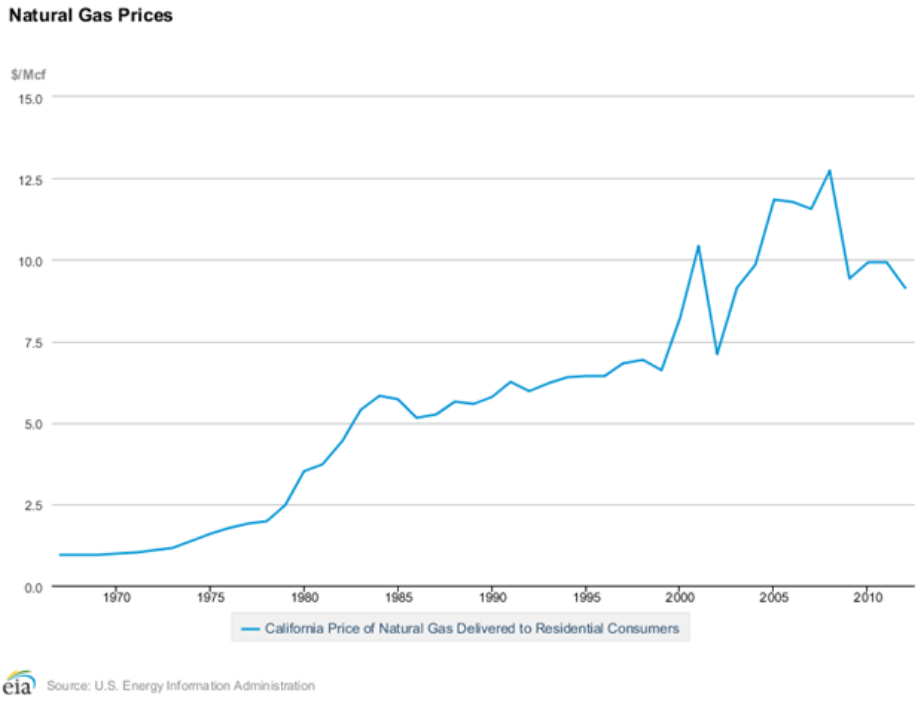

Source: United States Energy Information Administration, 2014

Changes in Design

To facilitate commercialization of the aluminum-based minichannel solar water heater systems, it may be necessary for the current design to undergo some changes. This would include potential changes to the collector, control logic and storage tank and associated piping.

Collector

A few aspects of the collector design can be improved for commercialization. The aluminum minichannel tubes used for the collector were obtained from stock available at the company Hydro and the tube dimensions were not optimized for maximizing heat transfer in a solar collector design. The dimensions of the tubes can be modified to increase heat transfer at a reasonable pressure drop of the working fluid by reducing the number of internal ports and slightly increasing the tube-minor dimension.

A follow-up version of the solar collector is currently being manufactured from copper minichannel tubes, which will allow steam generation. The design of the tube has been optimized to find a good compromise between heat transfer and pressure drop.

The prototype of the aluminum minichannel tubes were TIG welded to the aluminum header pipes. Ideally, the researchers want minimal space between the tubes to increase the area of the collector exposed to the solar irradiation. The separation of the tubes was defined based on the size of the nozzle for TIG welding, rendering a spacing of approximately 4 mm between tubes. Other manufacturing techniques, such as vacuum brazing or laser welding, could provide a reduction between tube separation and increase in throughput at commercial manufacturing plants.

Control Logic

The control logic used in the project was developed based on a research approach of maximizing the information provided by the data measurements. Standard commercial control logic and operation can be used with the minichannel solar collector.

Storage Tank and Piping

Likewise installing a flat-plate solar water heater system, the storage tank and piping will be varied depending of the size of the household and the design of the dwelling. However, the collector should be able to adapt to any of these changes.

Manufacturing Process

The manufacturing process of the aluminum-based minichannel solar water heater is primarily focused on the absorber, which includes the minichannel tubes and headers. After consulting an aluminum production company, the finalized design of the minichannel tube, required a die to be created for production. The company quoted approximately $20,000 per die, however hundreds of thousands of tubes can be created with a die. The process of producing the aluminum minichannel tubes goes through an extrusion technique called multi-port extrusions. Fortunately, this type of technique is not new; minichannel tubes, also known as microchannel

tubes, have been around longer in other industries such as in the HVAC, automotive and electronics cooling industries.

After producing the minichannel tubes, the next step is joining the tubes to the headers. The current prototype has the minichannel tubes TIG welded to the headers. However, it is ideal to minimize the spacing between the tubes to minimize heat loss. To minimize spacing and heat loss, other metal bonding technology such as furnace brazing should be used for minichannel fabrication. There are two popular types of furnace brazing techniques that are currently utilized for joining parts in heat exchangers in the automotive and HVAC industry: vacuum brazing and controlled atmosphere brazing (CAB). These techniques can be used to join the minichannel tubes with the headers and would minimize the tube spacing and thus tube heat loss. The benefits of either brazing techniques include control of precise tolerances, especially in very small spaces, and joining leading to clean joints with no additional finishing needed and both vacuum brazing and CAB share a similar fabrication process. Mass production of aluminum minichannel tubes joining with the header tubes will entail a continuous manufacturing line of equipment such as a degreaser, a fluxer if necessary, a brazing furnace and a cooling area (Szczurek et al., 2006; Zhao et al, 2013; Moller et al., 2014). Both techniques have some differences in process and finishes. Vacuum brazing has been around longer and been a preferred method for heat exchangers. The main differences between vacuum brazing and CAB is that vacuum brazing can handle alloys with a higher magnesium level (>0.3 percent), there is more process control in vacuum brazing, and it has a higher quality finish than CAB (Miller et al., 2000; GH Group, 2014; SECO/WARICK, 2011). The downside of vacuum brazing is that it can be more expensive than CAB (SECO/WARICK, 2011).

The collector frame and glass can easily be manufactured since it is similar to the glass and frame structures already used by traditional copper tube flatplate collectors. Indeed, the standard frame and glass used in today's flatplate solar collectors were purchased and used in the prototype minichannel solar collector. Additionally, everything else in the prototype system such as the piping and water storage tank is similar to those utilized in conventional solar water heating technology. There is no special attention that would be required.

Estimated Costs

Collector, Prototype Costs

The approximate total cost of the 10 ft. by 4 ft. aluminum minichannel solar collector is:

- Aluminum minichannel tubes from Hydro, $40 per tube, 11 tubes total = $440
- Headers, schedule 40 aluminum pipes, $14 per pipe, 2 pipes required = $28
- Collector frame and glass = $500
- TIG welding = $1,056
- Total = $2,024, or $50.6 per square foot.

Collector, Mass Production and Projected Costs

Because of extensive uses in extruded aluminum minichannel tubes in the automotive and HVAC industries, costs of mass production can be low especially for the more common sizes they produce. In general, extruded aluminum tubes are purchased by weight. For large volumes, extruded aluminum minichannel tubes can be purchased for $5 per kilogram depending on the value of aluminum in the market. If the prototype solar water heaters were to be mass-produced with the similar dimensions, the estimated costs are:

- Aluminum minichannel tubes for $5/kg; 11 tubes weighs about 9.809 kg = $49.09
- Headers, schedule 40 aluminum pipes, $14 per pipe (can be lower if purchased in bulk) = $28
- Collector frame and glass (can be lower if purchased in bulk) = $500
- Total costs of mass production per 10 ft. by 4 ft. aluminum minichannel solar collector = $577.04, or $14.43 per square foot.

It is noted the fabrication cost has not been considered; however, the cost of the collector is expected to remain below half of the current cost of a flat-plate collector.

Current Solar Water Heater and Installation Costs

Costs of installation size and costs in residential and non-residential sectors are shown in Table 4 and Table 5 and Figure 17 taken from (GTM Research and SEIA, 2011).

Table 4: Solar Water Heating Systems Average Price in 2011

	Residential $/sq. ft.	Non-Residential $/sq. ft.	Average Total Cost Residential	Average Total Cost Non-Residential
AZ	$232.82	$109.86	$8,847.24	$59,544.12
CA	$171.40	$109.40	$8,364.32	$116,953.90
CT	$138.40	$103.23	$11,830.71	$85,733.71
DE	$255.79	$234.20	$11,446.67	$29,978.00
MA	$156.31	$124.98	$11,371.14	$106,482.96
MD	$175.45	$117.48	$10,246.28	$18,796.80
MN	$157.91	$136.06	$11,416.89	$28,749.48
TX	$138.71	$141.67	$6,463.89	$25,500.60
VT	$152.55	$112.29	$10,144.58	$28,046.67
WI	$115.63	-	$15,575.36	-
National Average	$198.22	$111.78	$9,235.45	$82,165.14

Source: GTM Research and SEIA, 2011

GTM and SEIA reported in 2011 that average costs of SWH systems installed in residential sector of California was $8,364.32 for the entire system. In addition, the calculated average SWH system in the residential sector requires approximately 48.8 square feet. This gives an average costs per unit area of $171.40 per square foot. The system includes the cost of the

collectors, equipment such as the tank, pump, piping, etc., site design and labor. Tabulated costs of about 30 percent of the SWH system is solely the cost of the collectors. Using the numbers above, an average SWH collector costs $51.42 per square foot in the residential sector (GTM Research and SEIA, 2011).

Table 5: Average Solar Water Heating System Sizes in 2011 (square feet)

	Residential	Non-Residential
AZ	38.0	542.0
CA	48.8	1069.0
CT	85.5	830.5
DC	-	1,000.0
DE	44.8	128.0
MA	72.7	852.0
MD	58.4	160.0
MN	72.3	211.3
TX	46.6	180.0
VT	66.5	249.8
WI	134.7	-
National Average	50.2	530.0

Source: GTM Research and SEIA, 2011

Figure 17: Solar Water Heating Systems Breakdown Costs in 2011

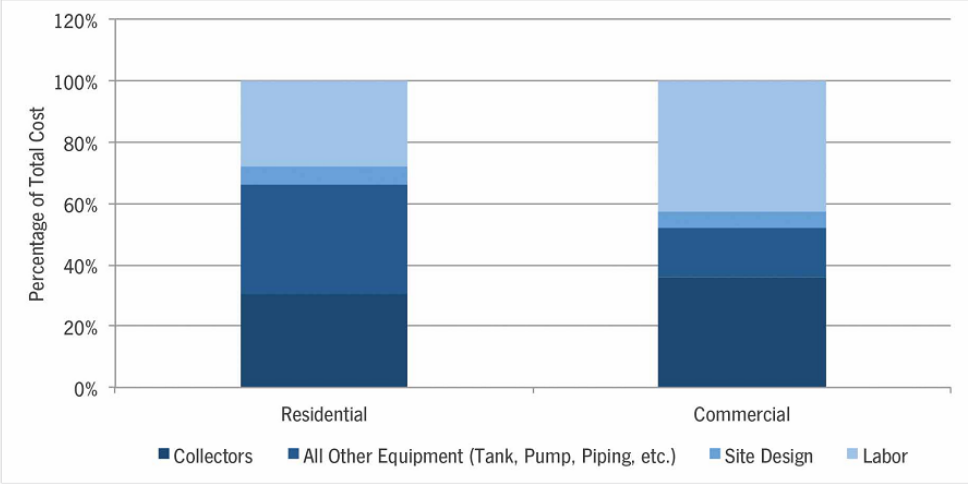

Source: GTM Research and SEIA, 2011

Likewise for the non-residential sector in California, the reported average SWH system cost is $116,953.90, with a mean system size of 1,069 square feet. This calculates to $109.40 per square foot. The report shows that about 35 percent of the total costs are the cost of the collectors alone, or about $38.29 per square foot (GTM Research and SEIA, 2011). Comparing the projected costs per unit area of the aluminum minichannel collector versus a SWH collector, substantial savings can be made in both residential and non-residential sectors.

CHAPTER 4:
Copper Minichannel Solar Water Heater

The second phase of the solar water heater project was to design, construct, and test a copper-based minichannel solar water heater. The extension of this project will test the possibility of a copper minichannel solar water heater to generate steam.

Copper Minichannel Collector Design

Although aluminum minichannels (also known as microchannels depending on their size) are a well-known technology in the automotive, HVAC and electronic-cooling industries, copper minichannel technology has yet to rise in popularity, mainly because only until recently, it was not possible to extrude copper. With only one group in the United States able to extrude copper into minichannels, the design of the copper minichannel tube has its limitations, especially with respect to the width of the tube that can be extruded. Dr. Frank Kraft at Ohio University has patented a technique of extruding copper minichannel tubes (Kraft, 2013). A brief overview of copper minichannel tube manufacturing can be found in Appendix A.

The first design copper minichannel considered is shown Figure 18.

Figure 18: Copper Minichannel Tube Design #1 (Millimeters)

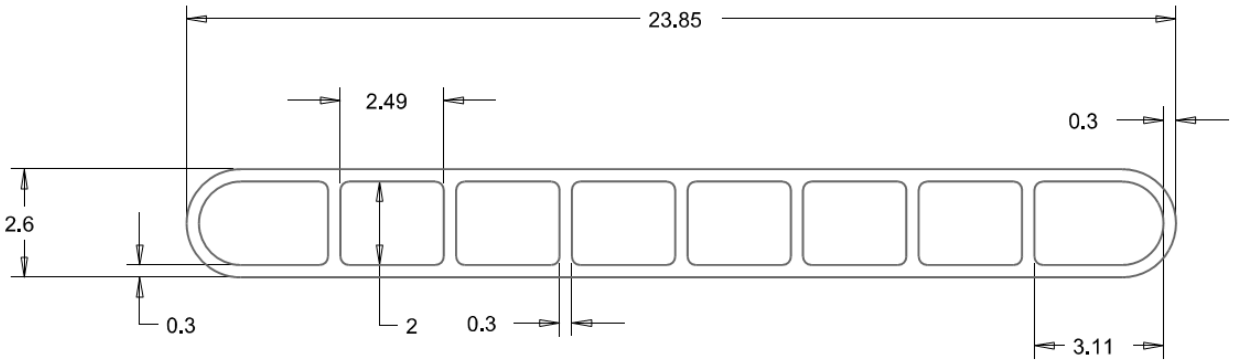

Source: University of California, Merced

However, due to restriction with respect to the width of this design, two other designs were suggested by Dr. Kraft. Design two and three are shown in Figures 19 and 20, respectively; design two has a smaller minor, or height of the minichannel tube, and design three essentially has the same height as design one but a smaller width.

Figure 19: Copper Minichannel Tube Design #2 (Millimeters)

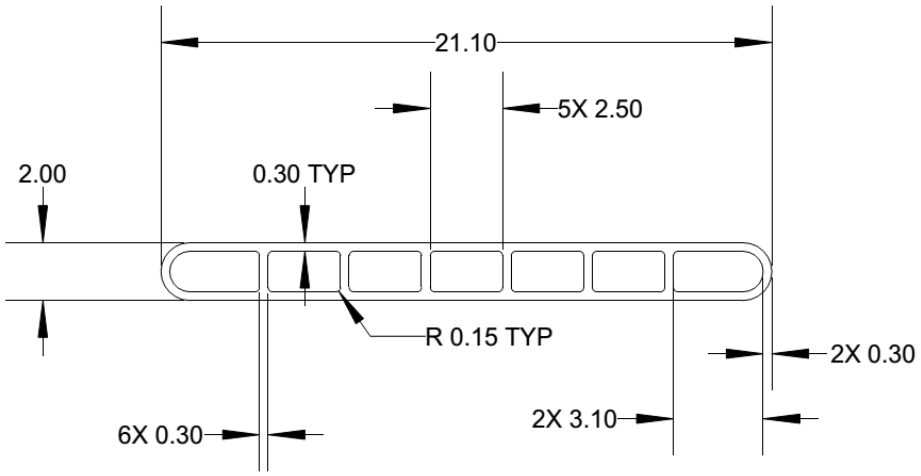

Source: University of California, Merced

Figure 20: Copper Minichannel Tube Design #3 (Millimeters)

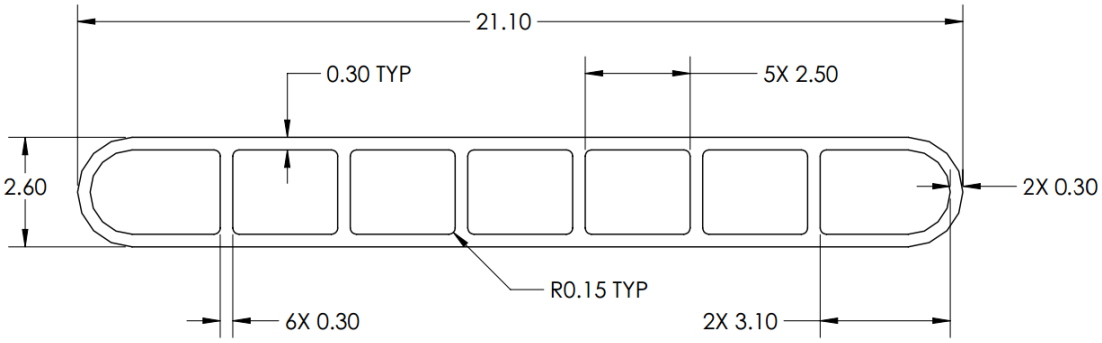

Source: University of California, Merced

Using the computational tool described in Chapter 1, the three designs were simulated as if they were used in a solar collector to compare tube performance. Comparing their performance can narrow down a design used to fabricate copper minichannel tubes for the copper minichannel solar collector. Appropriate dimensions, parameters and material properties of the copper minichannel tube were entered into the computational model. Some results that were compared to determine the final copper minichannel design are presented in Figure 21 through Figure 23.

Figure 21 compares Reynolds number and pressure drop in the three designs. Reynolds number is an alternative way of looking at flow rate, however, Reynolds number can also characterize whether the fluid is in laminar flow (Re < 2100) or turbulent flow. Pressure drop is an important parameter, and is basically the difference of pressure between two points. In this case, the pressure drop is calculated by computing the difference of pressure between the inlet and outlet of a minichannel tube. A higher pressure drop indicates more external power is needed to circulate the working fluid through the collectors. Design #2 signifies higher pressure drop as its Reynolds number compared to Designs #1 and #3. This is due to the minor, or

height, decrease in comparison to the other two designs. Both Design #1 and #3 exhibits similar behavior of increasing pressure as their Reynolds number is increasing.

Figure 21: Comparing the Three Reynolds Designs by Number versus Pressure Drop

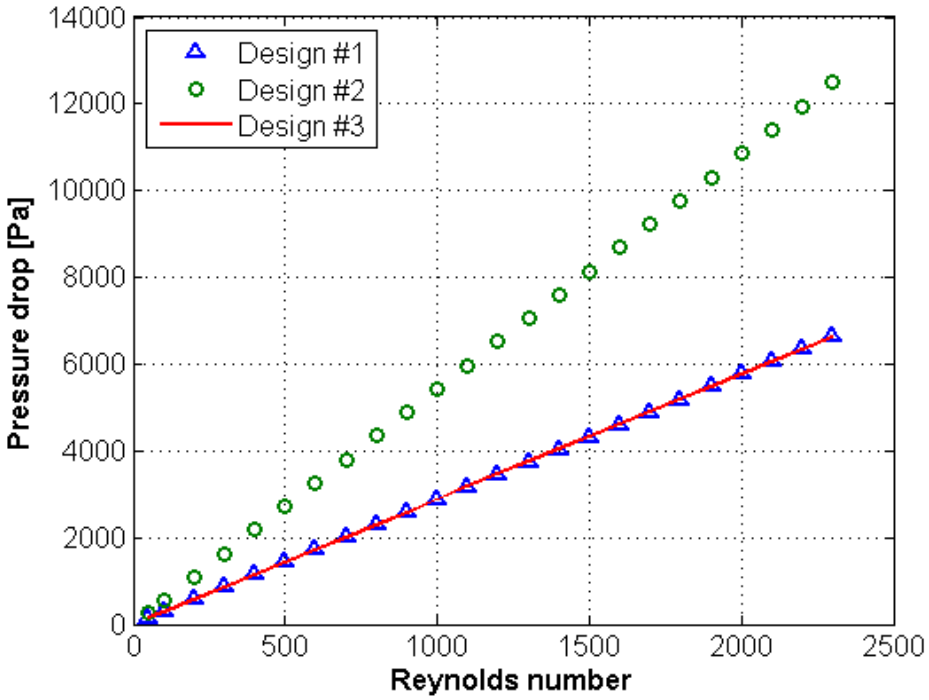

Source: University of California, Merced

Figure 22 compares Reynolds number and heat transfer of the three designs. The heat transfer is the rate that the minichannel tubes, acting as an absorber, collects the solar energy and transfers it to the working fluid. From plot shown, it looks like all the three designs exhibits similar performance with very little difference. It can be seen however that Design #2 shows smaller heat rate in the lower range of Reynolds number compared to Design #1 and Design #3.

Figure 23 simply combines the previous two figures together. Figure 23looks at the pressure drop and heat transfer of the three designs. It can be seen that while Design #1 and Design #3 exhibits similar performance and higher conduction heat transfer at lower pressure drops. Design #2 has lower conduction heat transfer rates in comparison to Design #1 and Design #3. This means that Design #1 and Design #3 are capable of achieving higher conduction heat rate at lower pressure drop, further concluding that Design #1 and Design #3 can achieve these conduction heat rates with lower required external power (that is, power from a pump).

From these results, since Design #1 cannot be used due the restriction of the width capable of being extruded, Design #3 was clearly the final design chosen to construct the copper minichannel solar collector. Twenty copper minichannel tubes were used for this design. The copper minichannel solar collector and system essentially uses the same type of components. The only difference is the sizing of the copper minichannel solar collector in comparison with the aluminum minichannel solar collector. Due to the width restriction of the copper minichannel tubes, the copper minichannel solar collector and system is smaller in size.

Figure 22: Comparing the Three Reynolds Designs by Number and Conduction Heat Transfer

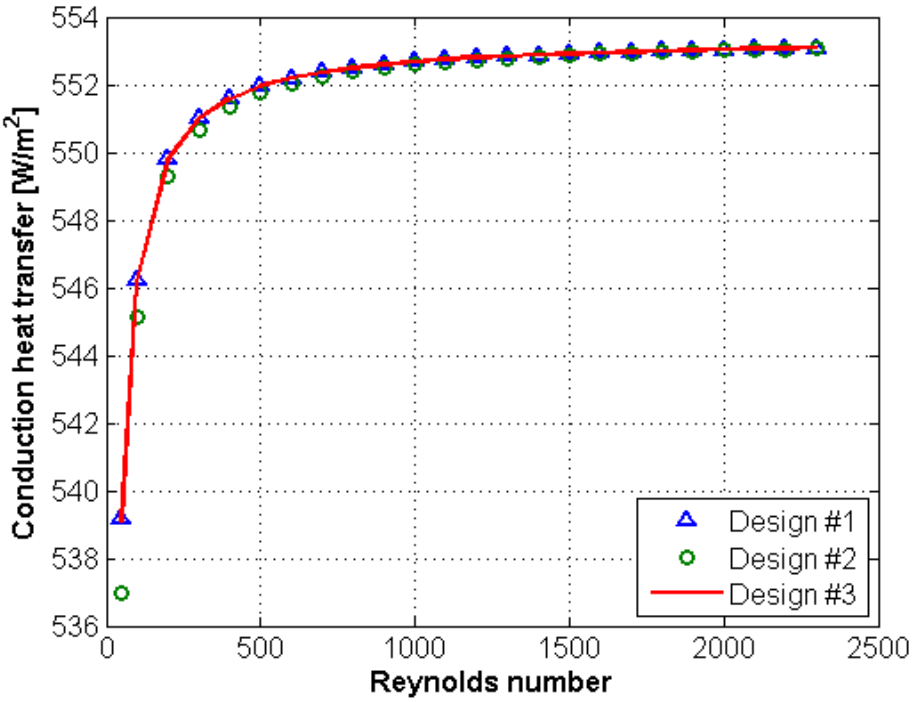

Source: University of California, Merced

Figure 23: Comparing All Three Designs by Pressure Drop versus Conduction Heat Transfer

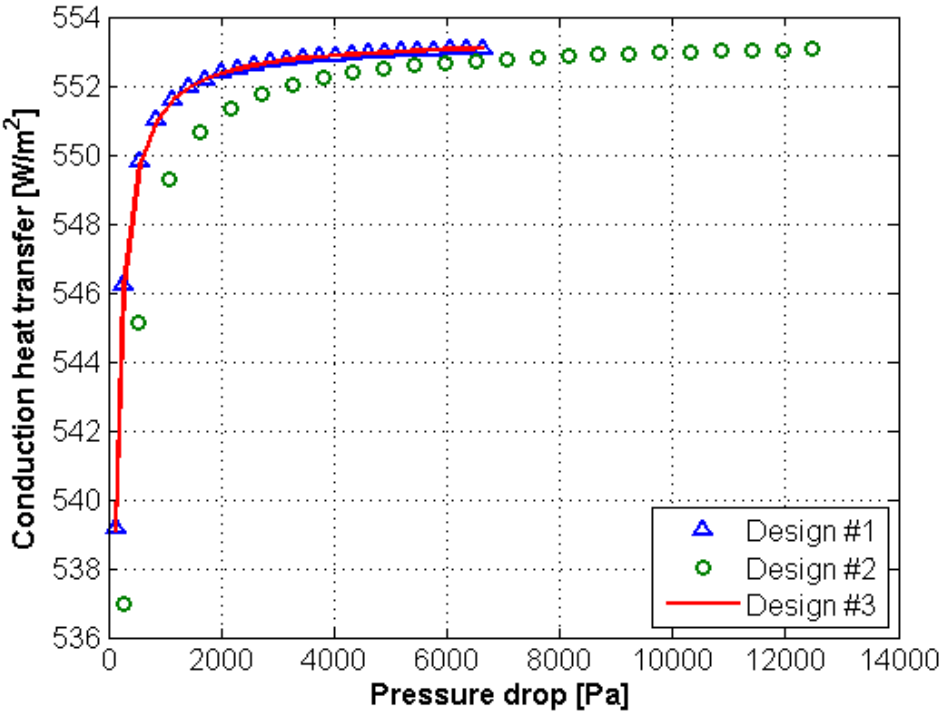

Source: University of California, Merced

Table 6 shows the dimensions of the copper minichannel solar collector, and Figure 24 gives a schematic and dimensions of the overall and final copper minichannel collector design.

Table 6: Dimensions of Copper Minichannel Solar Collector

	Copper Minichannel
Dimensions of Collector	
Frame length	1935.5 mm
Frame width	1021.1 mm
Absorber area	.756 m^2
Total free flow area	731.7 mm^2
Dimensions of Tube	
Hydraulic diameter of each tube	2.2 mm
Width (major)	21.10 mm
Height (minor)	2.60 mm
Length	1819 mm
Number of tubes	20
Port width	2.50 mm
Port height	2.0 mm
Wall thicknesses	0.30 mm
Number of ports	7

Source: University of California, Merced

Figure 24: Dimensions of the Copper Minichannel Tube Solar Collector

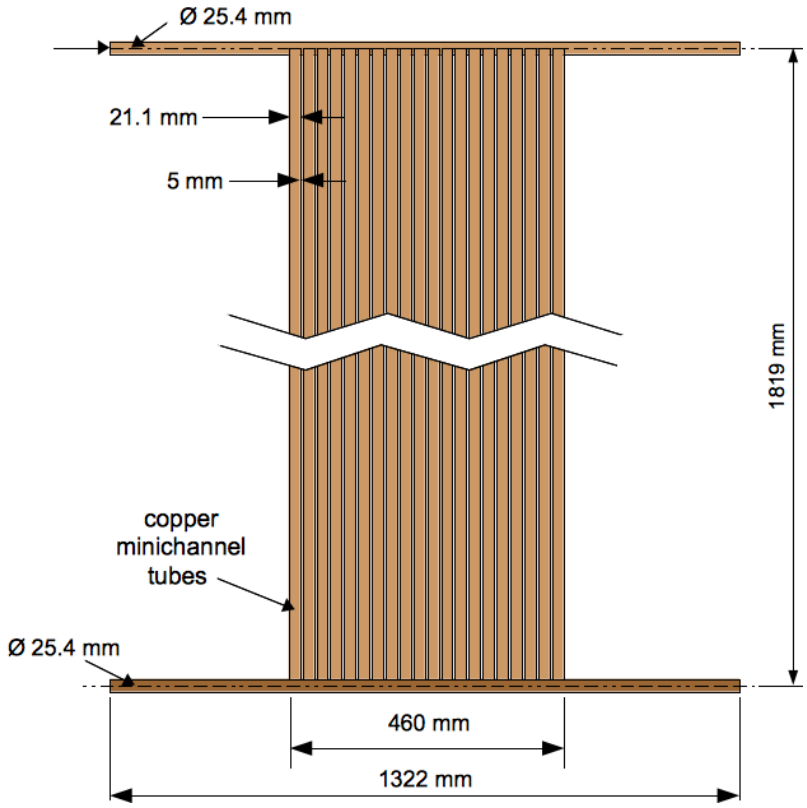

Source: University of California, Merced

Like the aluminum minichannel solar collector, the design of the copper minichannel collector included an inlet and an outlet header with the minichannel tubes inserted in between. Instead of TIG welding, the copper minichannel tubes were torched brazed to the headers. Torch brazing can allow two metals to join in small areas especially when precision is needed. Precision was required for the copper minichannel solar collector due to the fact that the walls of the copper minichannel tubes are thin and they are proned to melt if other metal joining techniques such as welding were used. In addition, joints created by torch brazing can operate at higher temperatures and perssure than ordinary soldering joints. This was needed since the copper minichannel solar collector was tested for potential steam generation.

After the copper minichannel tubes were torched brazed to the headers to form the solar collector, the collector was cleaned and a selective coating was applied. The selective coating used was the same that was applied on the aluminum minichannel and copper flat-plate solar collectors (Black chrome). Figure 25and Figure 26 show the copper minichannel solar collector before and after the application of the selective coating, respectively.

Figure 25: Copper Minichannel Solar Collector After Torch Brazing

Source: University of California, Merced

Figure 26: Copper Minichannel Solar Collector After Application of Selective Coating

Source: University of California, Merced

Once the selective coating is applied and allowed to dry, the copper minichannel solar collector was placed in a commerical metal frame like the aluminum minichannel and copper flat-plate solar collectors but with a smaller size. Figure 27 shows the final copper minichannel solar collector product ready to be connected with the system for testing.

Figure 27: Copper Minichannel Solar Collector in a Commercial Metal Frame Made for Conventional Solar Flat-plate Collectors

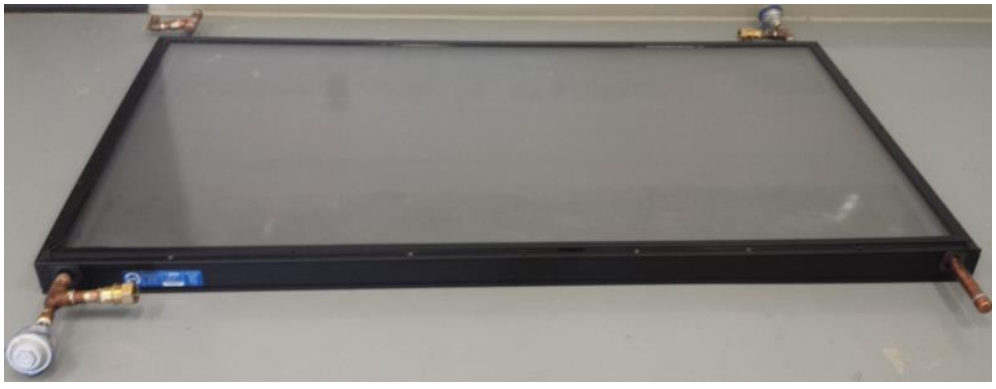

Source: University of California, Merced

System and Component Design

Although the copper minichannel solar collector shared similar types of components used in its system in comparison to the aluminum minichannel solar collector, the objectives of the copper minichannel solar collector is different and therefore the experimental design is different as well. The objectives of the copper minichannel solar collector is to analyze whether it can operate at a medium temperature range and possibly capable of generating low-grade steam. To gain more control of the collector and steam generation conditions, the copper minichannel solar collector was placed on a portable test stand instead of installing it stationary on a roof. This allows components of the copper minichannel solar collector to be accessible if adjustments or maintenance is needed. The test stand was built using aluminum T-slotted framing by 80/20.[7] The framing is basically structural aluminum bars with identical cross-sectional profiles ("T-slotted") that allows for easy fabrication (Figure 28).

Figure 28: Test Stand Fabricated for the Copper Minichannel Solar Collector

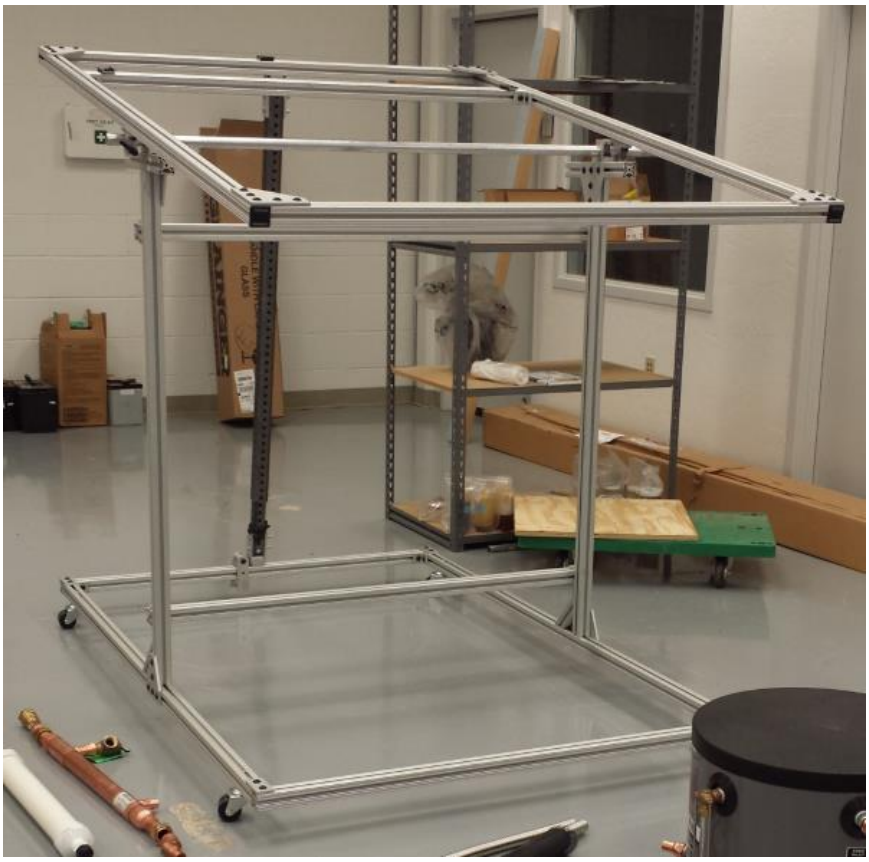

Source: University of California, Merced

The aluminum minichannel test stand and copper flat-plate solar water heater test stand use identical components such as the collector metal frame, data acquisition system, water storage tank, sensors and pump. Therefore, the components of the copper minichannel solar collector used similar components at a smaller scale because of the decreased size of the copper

[7] https://8020.net/university-tslot.

minichannel solar collector. There are a few components that are added to the copper minichannel solar collector system such as the steam generator apparatus and a cooling tank. A system diagram showing all the components of the copper minichannel system are shown in Figure 29.

Figure 29: Copper Minichannel Solar Collector System Diagram

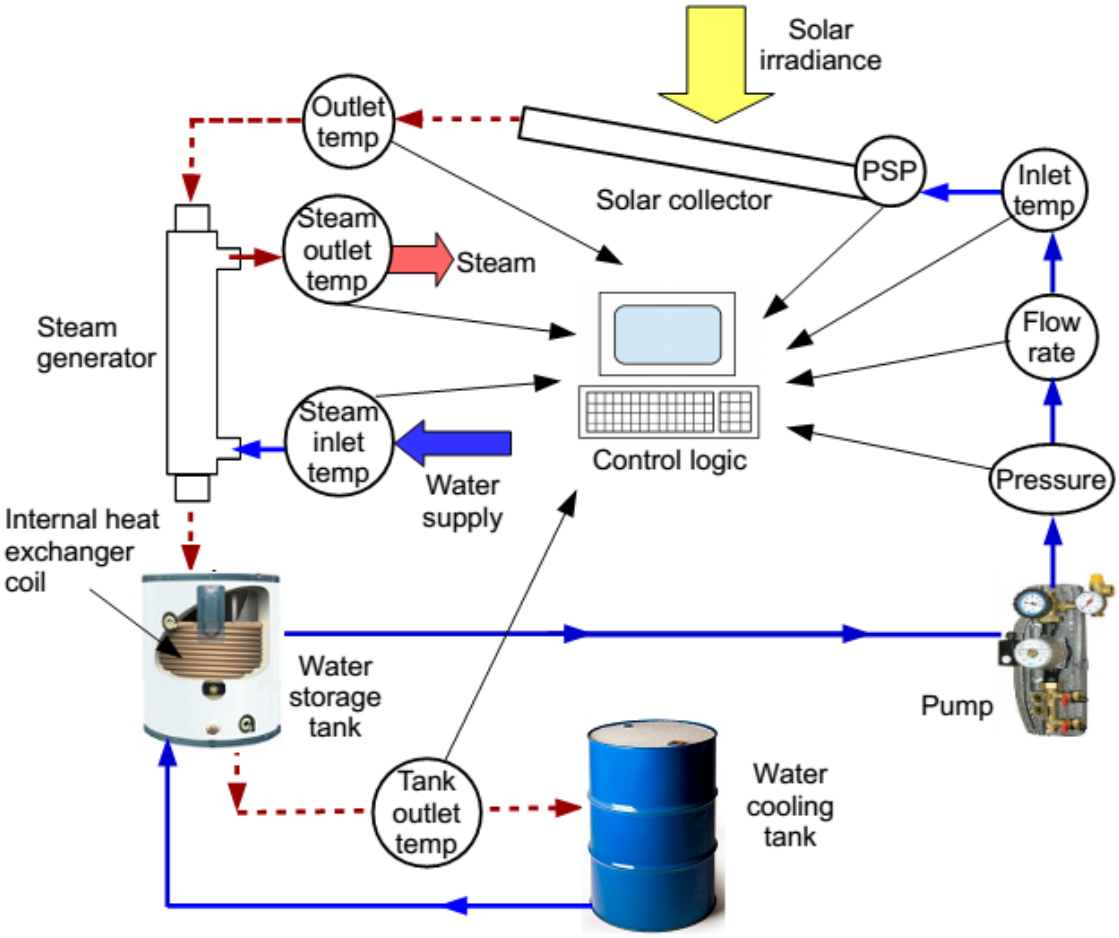

Source: University of California, Merced

The copper minichannel solar collector has the following main components: collector, pump, water storage tank, steam generator apparatus, cooling tank, and control logic (Figure 29). The sensors used in the test setup were; thermocouples to measure inlet, outlet, water storage tank outlet, and steam inlet and outlet temperatures; pressure transducer to measure pressure of the system; precision spectral pyranometer to measure the solar irradiance; and a volumetric flow meter to measure the flow rate of the working fluid circulating the system. Like the aluminum minichannel and copper flat-plate solar collectors, the copper minichannel solar collector collected data through a data acquisition system by National Instruments and programmed through LabView.

The working fluid used in the copper minichannel solar collector system is water passed through a water softener. The working fluid circulates from the water storage tank to the solar collector by an externally powered pump. In the copper minichannel solar collector, the working fluid absorbs the energy collected by the minichannel collector. Then, the working fluid circulates through the steam generator. The steam generator is a simple shell-and-tube heat exchanger where the working fluid is flowing through the internal tube while the concentric ("shell") external tube is filled also with water treated with a water softener, which absorbs the heat exchanged from the internal tube. As the water from the external shell tube is constantly gaining heat, the temperature rises and steam is generated. The working fluid from the internal tube of the steam heat exchanger then circulates to the water storage tank, and the working fluid cycles through the system again. The water storage tanks acts as a temperature control for the working fluid. If the working fluid is at an undesirable temperature, the cooling tank supplies cool water to reduce the temperature of the working fluid.

Test Results

Tests were performed during the first months of 2015 and after the end of the project. Results showed the copper minichannel solar collector can generate steam. The copper minichannel solar collector system was able to achieve self-pumping by operating in thermosyphon mode. Therefore, the constructed system was able to achieve steam generation temperatures without the use of external power from a pump. More details of the test results are shown in Appendix B.

CHAPTER 5:
Conclusions

The team tested (1) an aluminum based minichannel solar water heater, and (2) a copper minichannel solar collector for the purpose of generating low-grade steam.

The design uses the concept of minichannel tubes attached to headers and does not require a flat fin attached to the tube to transfer heat to the working fluid. The minichannel-based solar collector was constructed of aluminum, and its performance was compared to a conventional copper flat-plate collector, with the same external components and operating conditions. The team found the aluminum minichannel configuration to be 13 percent more efficient than a conventional copper collector, collecting more energy throughout the day.

To better understand the operation of the aluminum minichannel, the researchers developed and validated a mathematical model of the aluminum collector using test data from the project. The mathematical model shows that the lower thermal conductivity of aluminum does not translate into a loss of performance of the minichannel collectors when used in hot water systems. Even though aluminum does not conduct heat as well as copper, the aluminum system was able to heat the water just as well as a conventional copper collector.

The researches also designed, built and tested a copper minichannel solar collector for steam production. Rather than generating hot water, this solar collector was designed to generate low-grade steam. Efficacy testing of the copper steam system showed that when solar irradiance is 800 - 1,000 W/m^2 , the system can generate steam at a rate of about 2.4 to 2.8 g/min, with a solar absorber area of 0.757 square meters. Over two hours of operation, the copper minichannel tube collector increased the temperature of the working fluid within the collector to 100 - 115 degrees C. The data also shows the collector is capable of staying above 100 degrees C until late afternoon.

GLOSSARY

Term	Definition
Absorber	The part of a solar collector that absorbs the solar energy.
Flat-plate solar collector	A solar collector design that is basically a flat metal sheet with tubes evenly spaced and attached underneath the metal sheet. The metal sheet acts as a fin and solar absorber; the absorbed heat is transferred to the tubes underneath and transferred to the working fluid
Headers	The inlet and outlet tubes attached to the minichannel tubes. This is where the working fluid enters to and exits from the copper minichannel tube.
Heat exchanger	An apparatus that exchanges heat from one location to another.
Irradiance	Also known as solar irradiance. The amount of solar energy that is absorbed by Earth. It is measured by the solar power present on Earth by the unit area.
Selective coating	A coating applied to the collector to increase absorptivity.
Torch brazing	A technique of joining metals together by heating a filler metal to above melting point and with capillary action, the filler metal is distributed between the metals
Working fluid	The fluid contained in the solar collector and cycled through the solar collector system. This fluid absorbs the heat transferred from the solar collector.

LIST OF ACRONYMS

Acronym	Definition
CAB	Controlled atmosphere brazing
CPUC	California Public Utilities Commission
kG	Kilogram
kN	Kilonewton, a unit of force
Mcf	Million cubic feet
SEIA	Solar Energy Industries Association
SWH	Solar water heater
TIG	Tungsten inert gas
W/m2	Watts per square meter

REFERENCES

Cassard, Hannah; Denholm, Paul; Ong, Sean. Break-even for residential solar water heating in the United States. National Renewable Energy Laboratory. Contract 303-275-3000.

CPUC. Review of the incentive levels and progress of the California solar initiative-thermal program. Technical report. California Public Utilities Commission, Energy Division, Customer Generation Programs. 2014. From http://www.cpuc.ca.gov/NR/rdonlyres/B7D3D1AC-5C9A-49C9-81E1-8E03E471AA73/0/CSIThermalAB2249ReportFinalWebVersionJanuary292014.pdf

Diaz, Gerardo. Performance analysis and design optimization of a mini-channel evacuated-tube solar collector. In proceedings of ASME IMECE, Paper # IMECE2008-67858. 2008.

Diaz, Gerardo. Experimental characterization of an aluminum-based minichannel solar water heater. In proceedings of the ASME 2013 Summer Heat transfer Conference, July 14-19, Minneapolis, USA. Paper #HT2013-17347. 2013.

EES. Engineering Equation Solver. F-Chart Software. 2014. < http://www.fchart.com/ees/>

Energy.gov. Tax credits, rebates and savings | Department of Energy. 2014. From http://energy.gov/savings

GH Group-Induction Atmosphere. Types of Brazing Atmosphere. 2014. From http://www.gh-ia.com/brazing/atmosphere-types.html

GTM Research and SEIA. U.S. solar market insight report: 2011 solar heating and cooling year-in-review. Technical report. GTM Research Solar Analysts, SEIA Policy and Research Division. 2012.

Hudon, K.; Merrigan, T.; Burch, J.; Maguire, J. Low-cost solar water heating research and development roadmap. National Renewable Energy Laboratory. Contract 303, 275-3000. 2012.

Kemp, Clarence M. Apparatus for utilizing the sun's ray for heating water. U.S. Patent No. 451,384. 1891.

Kraft, Frank. Micro-channel tubes and apparatus and method for forming microchannel tubes. CA Patent No. 2,672,098. 2013.

Miller, W.S.; Zhuang, L.; Bottema, J.; Witterbrood, A. J.; De Smet, P.; Haszler, A.; Vieregge, A. Recent development in aluminum alloys for the automotive industry. Materials Science and Engineering: A, 280(1), pp. 37-49. 2000.

Moller, Craig; Grann, Jim. What matters most in vacuum aluminum brazing. Welding Journal, 93(2), 50-60. 2014.

Murray, Ed. U.S. solar thermal market outlook. Powerpoint slides. California Solar Energy Industries Association, Aztec Solar, Inc. and ELM Distribution. 2010. From http://solarthermalworld.org/content/us-solar-thermal-market-outlook-2010

Newport Partners. Comparing residential water heaters for energy use, economics and emissions. Tech. report. Propane Education and Research Council, Davidsonville, MD. 2011.

Proske, Frank. Solar thermal energy and market trends. Powerpoint slides. A.O. Smith Water Products Co., Meshoppen, PA. 2010. From http://solarthermalworld.org/content/solar-thermal-energy-technology-and-market-trends-2010

Robles; Azucena; Duong, Van; Martin, Adam J.; Guadarrama, Jose L.; Diaz, Gerardo. Aluminum minichannel solar water heater performance under year-round weather conditions. Solar Energy, 110, pp. 356-364. 2014.

SECO/WARWICK. Controlled atmosphere aluminum brazing systems. Product pamphlet. 2011. From http://www.secowarwick.com/assets/Documents/Brochures/Controlled-Atm-Alum-Brazing-Systems.pdf

SEIA. Solar heating and cooling. Powerpoint Slides, Solar Energy Industries Association. 2013.

Sharma, Neeraj; Diaz, Gerardo. Performance model of a novel evacuated tube solar collector based on minichannels. Solar Energy, 85, pp. 881-890. 2011a.

Sharma, Neeraj; Diaz, Gerardo. Minichannel tube solar collector. US patent application US 2011/0186043 A1. 2011b.

Sustainable Thermal System Laboratory. Design of air-cooled microchannel condensers for mal-distributed air flow conditions. Georgia Institute of Technology: Atlanta, GA. From http://stsl.gatech.edu/research-aircoupled.html

Szczurek, Janusz; Kowalewski, Janusz. Issues in vacuum brazing. In Brazing and Soldering: Proceedings of the Third International Brazing and Soldering Conference, April 24-26, 2006, San Antonio, TX, ASM International, pp. 326.

Weather Underground. Historical weather: weather history for Atwater, CA 95301. 2014. From http://www.wunderground.com/history/

U.S. Energy Information Administration. Natural gas: natural gas process. 2014. From http://www.eia.gov/dnav/ng/ng_pri_sum_dcu_nus_a.htm

Zhao, Hui; Elbel, Stefan; Hrnjak, Pega. Controlled atmosphere brazing aluminum heat exchangers. Welding Journal, 92(2), pp. 44-46.

APPENDIX A:
Copper Minichannel Tube Manufacturing

The following information was shared by Dr. Frank F. Kraft of Ohio University. All photos were provided by and credited to Dr. Frank. F. Kraft.

The components and parts needed for extrusion, such as the container, ram-stems, dummy blocks, and extrusion dies were fabricated from ATI 720, Inconel 720 and Rene 41 which all are nickel-based superalloys to withstand high extrusion temperature. Figures A-1 and A-2 below shows photos of the extrusion die and ram-stems.

Figure A-1: Extrusion Die

Container with extrusion die inside; minichannel die profile is seen inside

Source: Dr. Frank. F. Kraft

Figure A-2: Extrusion Die and Ram-stems

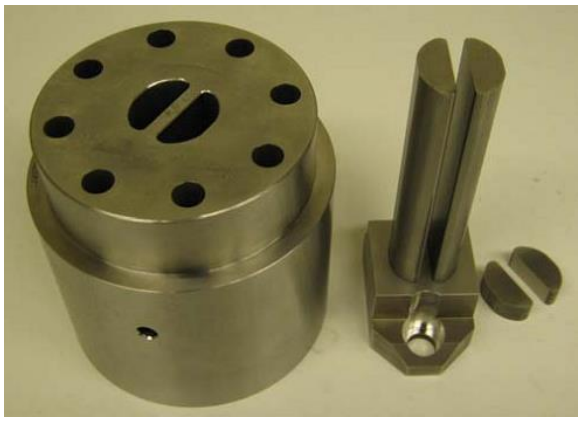

Container with extrusion die inside (left); ram-stems (right)

Source: Dr. Frank. F. Kraft

The extrusion components are assembled on a servo-hydraulic (model 810 MTS®) machine that is capable of producing 250 kN of ram force. Cartridge heaters are inserted into the container where the entire apparatus is insulated with a zirconia “blanket” prior to extrusion. Zirconia is a ceramic also known as zirconium dioxide, a white crystalline oxide of zirconium. Photos of the servo-hydraulic 810 MTS® machine are shown in Figure A-3.

Figure A-3: Servo-hydraulic 810 MTS® Machine

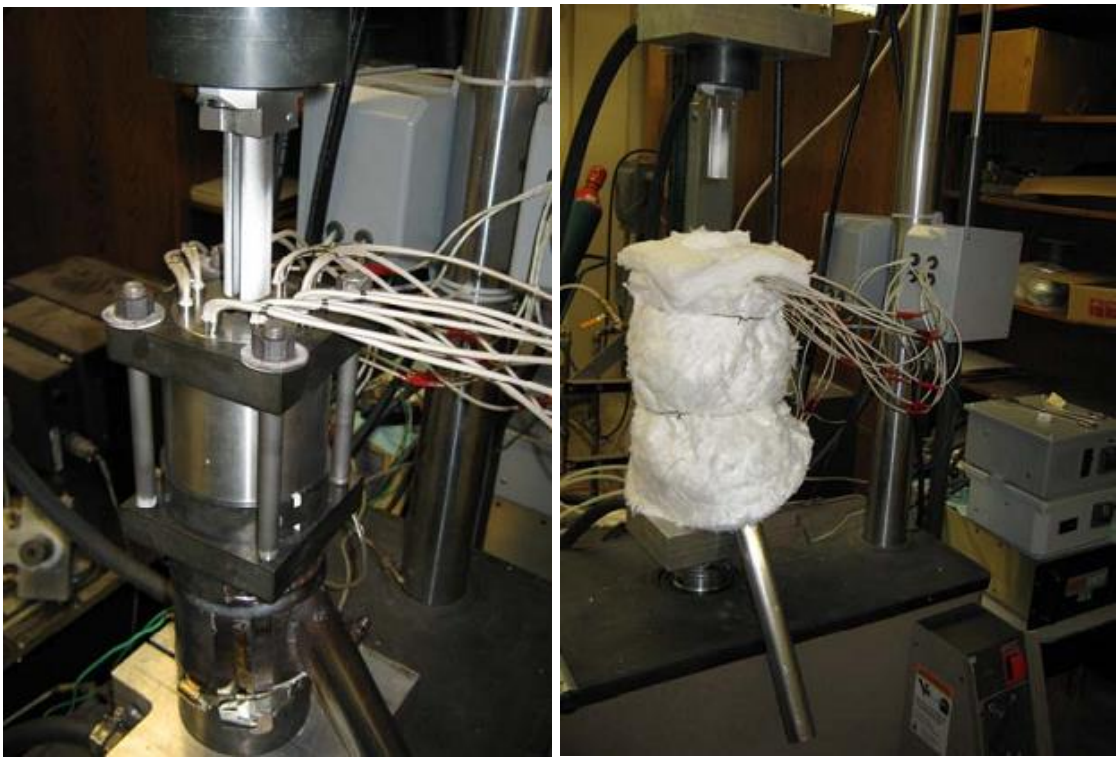

All components assembled together on the MTS® machine (left); assembled components wrapped in zirconium dioxide blanket (right).

Source: Dr. Frank. F. Kraft

Extrusion billets were machined from OFHC 101-Cu copper rods to fit into the container. To fulfill the design requirements and constraints, the container bore dimensions were important due to the following factors: 1. Width of the tube, 2. Buckling criteria of the ram stems, 3. The ram pressure required for extrusion, 4. The force limitations of the MTS® machine, and 5. The billet volume required to produce the desired tube length plus the discard lengths at the beginning and end of the extrusion. For this particular project, 1819 mm in length was the desired tube length and 42 total billets were used. The copper billets are presented in Figure A-4 as well as the billets machined to fit in the container.

While the copper billets are heated in the apparatus, the MTS® machine provides the ram with enough force (up to 250 kN) to push the copper billets through the die. The product, or minichannel tube, exits the heated extrusion through a nitrogen gas-tube that is attached to the lower part of the apparatus. The apparatus is shown in Figure A-5.

Figure A-4: Copper Billets

Copper billets (left), and copper billets machined to fit the container (right).

Source: Dr. Frank. F. Kraft

Figure A-5: Copper Extrusion Apparatus

Extruded copper minichannel tube exiting from the nitrogen gas-tube located at the lower part of the apparatus (left); closer view of the nitrogen gas-tube on the apparatus (right).

Source: Dr. Frank. F. Kraft

After the copper minichannel tubes are extruded from the apparatus, the tubes were straightened in both planes and cut to the desired length. The photos in Figure A-6 shows the finished product.

Figure A-6: Finished Product

Finished product measured (left), copper minichannel tube straightened (center), and copper minichannel tubes packaged with aluminum angle supports.

Source: Dr. Frank. F. Kraft

After each extrusion, the apparatus was allowed to cool to room temperature before it was disassembled. The remaining copper in the die was removed by using an Instron® test machine by pulling it from the die. A special fixture was constructed for this purpose. Lastly, the residual copper in the container and die was dissolved in nitric acid under a fume hood. Aftermath of the container and die, and an Instron® machine in process of removing the remaining copper are shown in Figure A-7.

Figure A-7: Container, Die and Instron® Machine

Residual copper in the container and die (left); Instron® machine removing the residual copper from the die (right).

Source: Dr. Frank. F. Kraft

APPENDIX B:
Copper Minichannel Solar Collector Test Results

Test results obtained with the copper minichannel solar collector are shown below. Figure B-1 shows that the copper minichannel solar collector can achieve 100 ˚C and above for steam generation conditions, as shown by the dashed-green line denoting the outlet temperature of the collector. The solar irradiance of during the test was relatively steady for half of the day and started to decrease towards the afternoon, the temperatures at the collector inlet and outlet continued to increase throughout the day. Right after 4:00 PM, it is seen that the collector reached temperatures a few degrees higher than 100 ˚C and stayed at that operating conditions for more than half an hour. The spikes in temperature at the outlet of the collector between 11:00 AM and 12:30 PM and between 2:00 PM and 3:00 PM were due to stagnation conditions, that is the pump was turned off. This shows that the stagnation temperature of the collector reaches around 113 ˚C.

Figure B-1: Copper Minichannel Solar Collector Testing on April 30, 2015

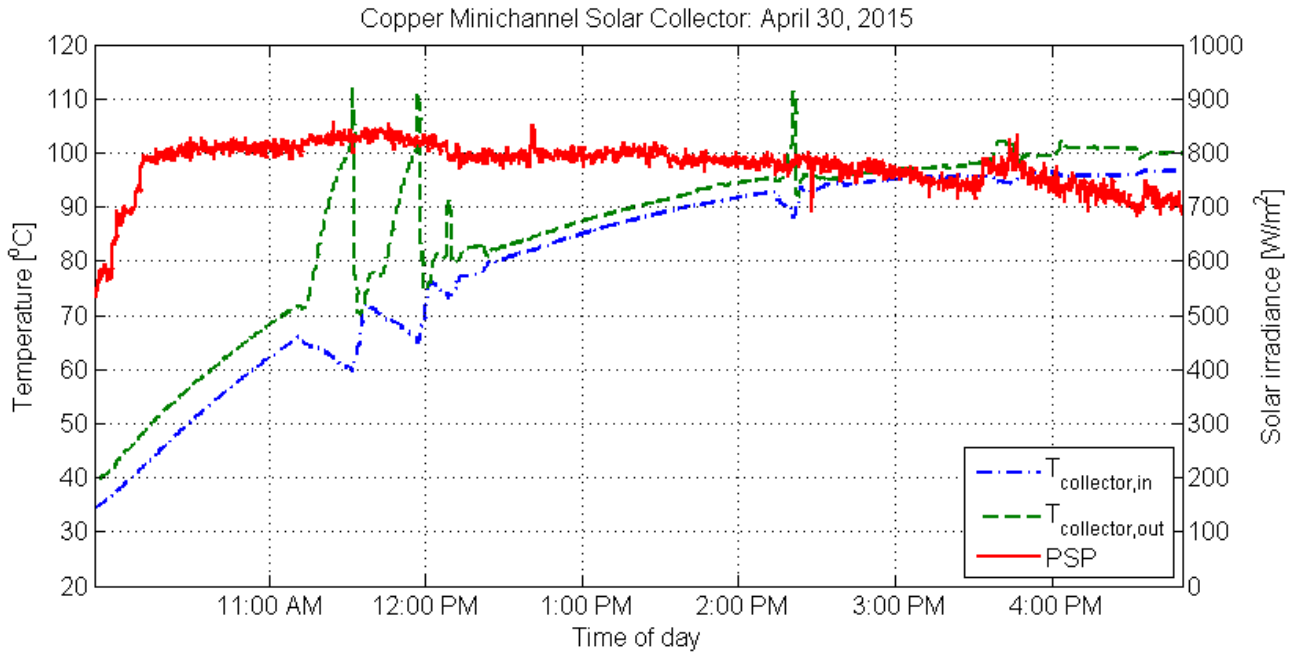

Source: University of California, Merced

Operating conditions in thermosyphon mode can be observed in Figure B-2, where the solid black line denotes the volumetric flow rate through the closed loop. The collector was able to self-pump and circulate the working fluid through the collector without the use of an externally-powered pump, although the variability of the solar irradiance and the temperature differences in the loop made hard to control in thermosyphon mode. From Fig. B2, at around

1:30 PM, it can be seen that the pumped is turned off by the decreasing values of the temperatures, resulting in a flow rate falling to zero. However, addition of tap water to the inlet of the heat exchanger cold section allowed the flow to start again, which was recorded at around 1:40 PM where the flow rate jumped from zero to about 1 liter per minute. The self-pumping lasted about 20 minutes until the temperature difference dropped and the flow stopped again. Addition of more water resulted in the self-pumping mode starting again at around 2:10 PM which lasted for about 20 minutes.

Figure B-2: Copper Minichannel Solar Collector Testing on April 30, 2015

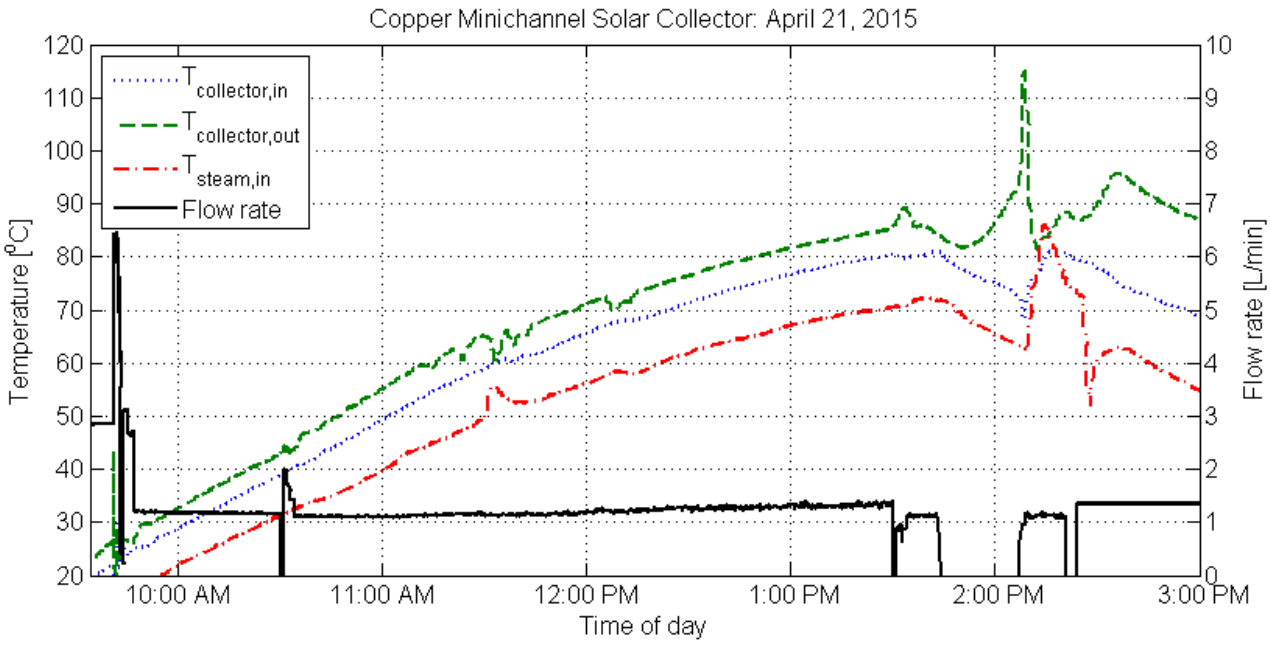

Source: University of California, Merced

Figure B-3 shows another instance when the thermosyphon mode can be observed. Around 12:40 PM, it can be seen that the pump is turned off resulting in a decrease in the flow rate from about 2.8 liters per minute to 1.3 liters per minute. It can also be seen that the collector inlet temperature decreases rapidly. The system is self-pumped from 12:40 PM to about 1:15 PM, after which the pump is turned back, and an increase spike can be seen by the collector inlet temperature. The temperature difference between inlet and outlet collector temperature is usually less than 5 degrees Celsius, but the difference increases significantly when the pump is turned off and the system works in thermosyphon mode. The two by-pass valves can be used to control the flow rate inside the closed loop system. The water inlet port of the heat exchanger cold side can be used to maintain a flow during thermosyphon conditions.

To calculate the steam generation rate, the amount of water filling the outer shell of the steam heat exchanger was initially recorded by using the rotameter and marking the start and end fill lines on the sight glass as seen in Figure B-4.

Figure B-3: Copper Minichannel Solar Collector Testing on May 12, 2015

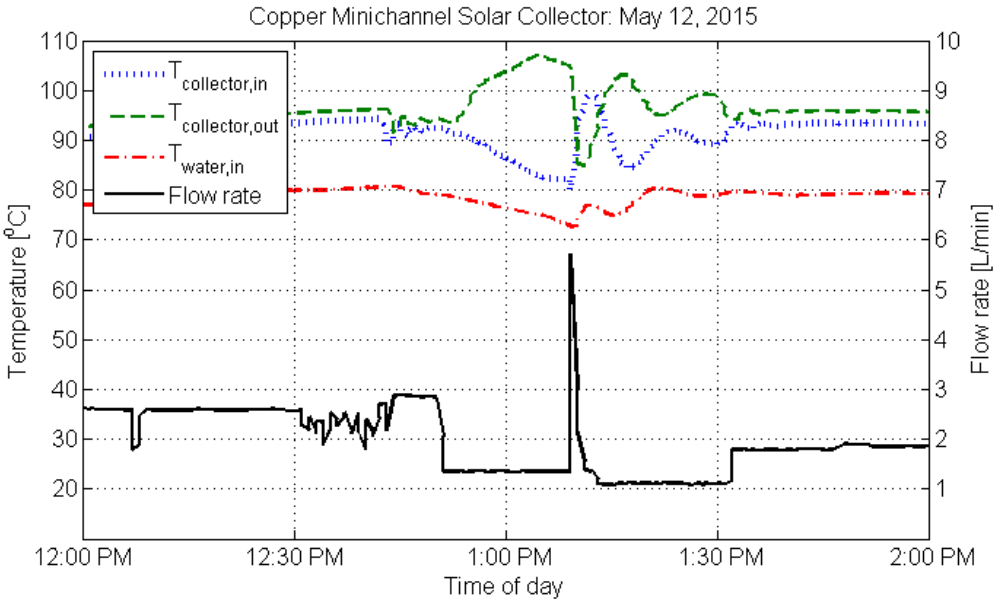

Source: University of California, Merced

Figure B4: Sight Glass to Determine Steam Generation

Source: University of California, Merced

The sight glass detects the water level or amount of water in the outer shell. The rotameter reads the rate of water in volume per time entering into the outer shell. By allowing the rotameter to read a constant flow rate and taking the time the water level took to reach the end mark, the volume of water in the outer shell of the steam heat exchanger can be calculated. Once steam is generated, time is recorded to analyze the time it takes the water level in the sight glass to reach the starting level mark. The rate of steam generation is calculated by dividing the volume of water of the outer shell of the heat exchanger by the time it takes the water level to reach from the end to the start marks of the fill. Then multiply that volumetric flow rate by the density of saturated steam. Several calculations were made and the steam generation rate for the limited testing period of the copper minichannel solar collector was in the range of 2.4 to 2.8 g/min.

From Figure B-5(a) it is observed that the outlet temperature of the steam generator, T Steam, starts the test at around 30 [°C] and at around 8000 seconds it sharply increases its value to reach boiling temperature at atmospheric conditions. Also shown are the inlet and outlet temperatures to the solar collector, the ambient temperature, and the volumetric flow rate. In Figure B-5(b), the solar irradiance obtained with a precision spectral pyranometer is shown. The steam generation efficiency was calculated at around 18 percent and thermosiphon operation was detected by turning off the external pump and verifying continuous flow rate with the rotameter.

Figure B-5: Steam Generation with the Copper Minichannel Solar Collector

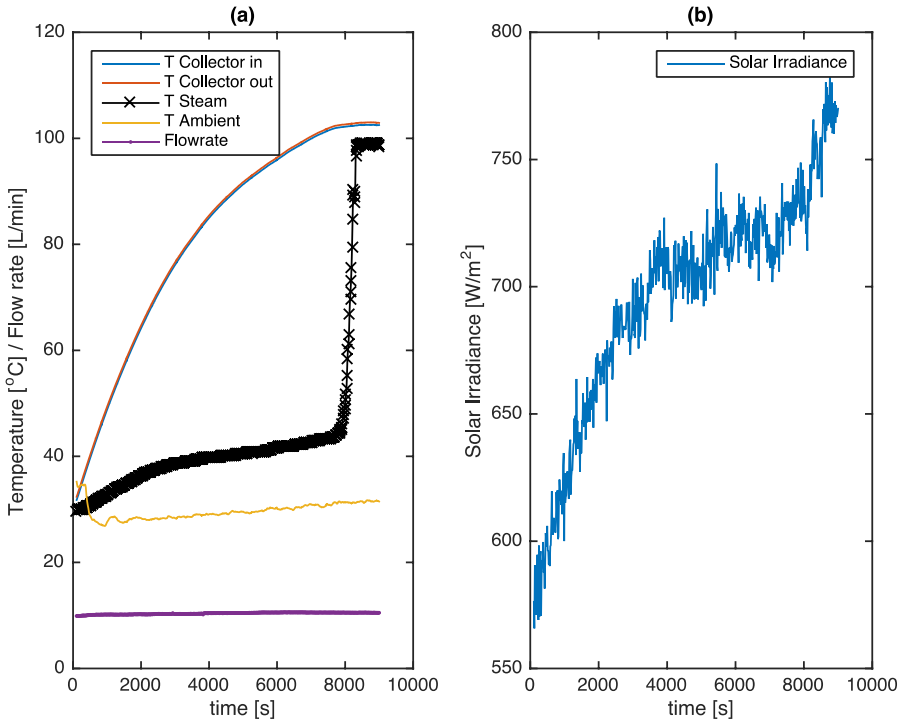

Source: University of California, Merced

APPENDIX C:
Test Plan and Sample Test Data

Test Plan Aluminum Collector

A closed loop configuration was utilized with a mixture of 50 percent propylene glycol and 50 percent water by volume. The propylene glycol mixture exchanges energy with water inside the storage tank by means of an internal coil heat exchanger. A standard commercially available 80-gallon (302.8 liters) water storage tank from SunEarth Inc. was used in the installation. Although the thermophysical properties of the glycol mixture are inferior to water, the mixture allows operation of the system at below-freezing ambient conditions minimizing the chances of bursting tubes due to ice formation inside the tube ports. A 1/4 HP Grundfos pump was used to move the working fluid around the closed loop system.

Data were collected with a National Instruments CompactDAQ system connected to LabVIEW which recorded inlet and outlet temperatures at the collector, as well as, water temperature inside the storage tank. Type K thermo- couples with a range between −200 ˚C to 1250 ˚C from Omega were utilized which have a standard limit of error of 1.1 ˚C over the entire scale. The volume flow rate through the water heater was measured with a Grundfos low-flow sensor Model # VFS 1-20 with an accuracy of 1.5 percent of the full scale, and the solar irradiation was measured with a precision spectral pyranometer from Eppley installed on the same plane as the collector. The solar water heater was installed on the roof of the laboratory building at the University of California at Merced with geographic coordinates of +37˚22’ 28.59” and -120˚34’ 38.10” , which has an angle of 18˚ with respect to the ground. The flow through the collector between inlet and outlet was oriented North-to-South. The system was controlled directly from LabVIEW with the close loop pump being turned on when the precision spectral pyranometer signal was greater than 150 W m^{-2}. For safety reasons, the discharge valve from the storage tank was automatically controlled to open whenever the temperature inside the tank reached 55 ˚C allowing cold water from the water supply to flow into the water tank, lowering its temperature. The discharge valve remained open until the temperature inside the tank fell below 30 ˚C. At this point, the discharge valve was closed and the water temperature inside the storage tank was allowed to rise again due to the exchange of energy with the glycol mixture flowing through closed loop.

The variables recorded included:

- Date
- Elapsed Time (s)
- Temp_in_Al (deg C)
- Temp_in_Cu (deg C)
- Temp_out_Al (deg C)
- Temp_out_Cu (deg C)

- Temp_Tank _Al (deg C)
- Temp_Tank_Cu (deg C)
- Flowrate_Al (L/min)
- Flowrate_Cu (L/min)
- PSP (W/m^2)
- Temp_Flowmeter_Al (deg C)
- Temp_Flowmeter_Cu (deg C)
- Valve_Al_Tank_Discharge (V)
- Valve_Cu_Tank_Discharge (V)
- Pumps

Test Data

The spread sheets with sample test data for two days, that is, February 13, 2014 and June 21, 2013, which represent very different ambient and solar irradiance conditions, are provided in Appendix C.1 (publication number CEC-500-2019-008-APC-1) and Appendix C.2 (publication number CEC-500-2019-008-APC-2), both available at www.energy.ca.gov.

APPENDIX D:
How Equations in Chapter 1 were Derived

Single-Phase Flow Mathematical Model

This appendix presents the mathematical formulation developed to predict the performance of aluminum and copper minichannel solar collectors operating at single-phase flow. The mathematical model is based on the one-dimensional energy balance equations. The single-phase mathematical model is compared and validated against the experimental results of the aluminum minichannnel solar collector.

Single Phase Flow

Glass Cover

An energy balance is applied at the glass cover as seen in Figure 3.1. The energy balance includes the solar irradiance, radiation heat transfer exchange between the absorber and the glass, convection heat transfer between the absorber and the glass, and the losses due to the convection to the ambient air, radiation to the sky, and glass transmissivity:

$$q_{in} + q_{rad,air-g} + q_{conv,g-air} = q_{conv,g-sky} + q_{rad,g-sky} + q_{absorbed} \text{ or}$$

writing out the heat fluxes in the respective order,

$$G_s + \left(\frac{1}{\frac{1}{\text{-}} + \frac{1}{(T} - } \right) \sigma \left(T_{abs}^4 - T_g^4 \right) + h_{air} \quad _{air} - T_g \right) \tag{3.1}$$

$$= h_{4} \quad _{g,air} (T_g - T_{\infty}) + E_g \sigma \left(T_g^4 - T \right. \quad + \left(\frac{\alpha_{abs} \tau_g}{1 - (1 - \alpha_{abs})(1 - \alpha_g)} \right) G_s$$

Figure D-1: Energy Balance of Minichannel Tubes Solar Collector

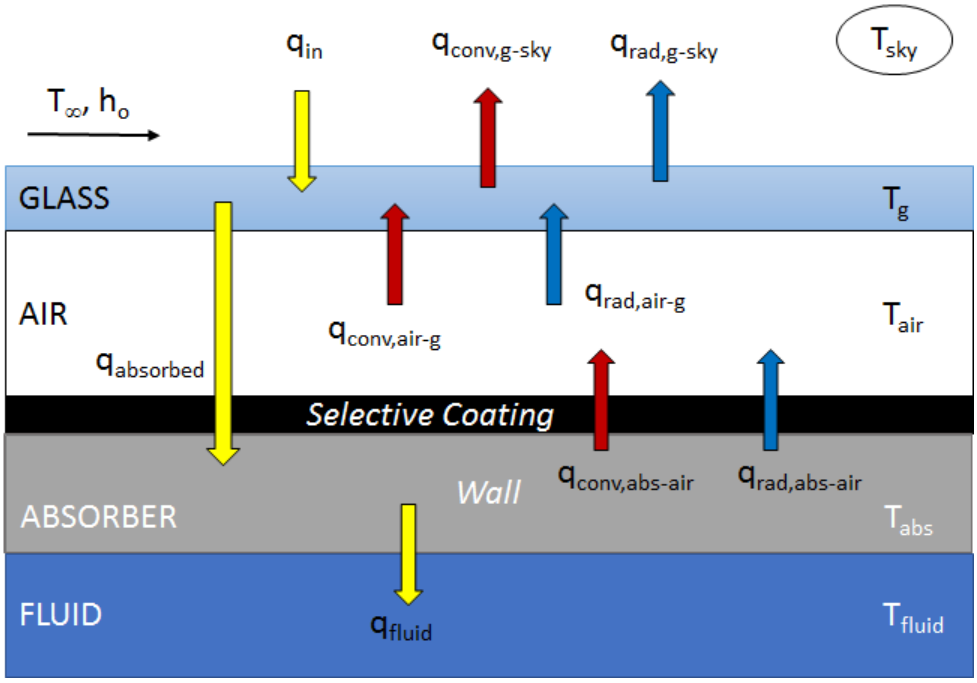

Source: University of California, Merced

On the left-hand side of Eq. 3.1, G_S is the total solar incident radiation, E_g is the emissivity of the glass cover, E_{abs} is the emissivity of the absorber, σ is Stefan- Boltzmann constant, T_{abs} is the temperature at the absorber, T_g is the temperature at the glass, hair is the convection heat transfer coefficient of the air between the glass and absorber, and T_{air} is the temperature of the air between the glass and absorber. On the right-hand side, T∞ is the temperature of the ambient air, αabs is the absorption coefficient of the absorber, τg is the transmissivity of the glass, and ρg is the reflectivity of the glass. hg,air represents the convection heat transfer coefficient between the glass cover and the ambient air given as an empirical expression from Fonseca and Khoukhi and Maruyama [31, 32]:

$$h_{g,air} = 2.8 + 3v_{wind}$$

where vwind is the velocity of the ambient air in (m/s). Tsky represents the sky temperature in relationship with the ambient temperature, T∞, and is also an empirical equation given by Khoukhi and Maruyama [32]:

$$T_{sky} = 0.552 T_{\infty}^{1.5}, \qquad (K)$$

Absorber-Cover Gap

For the gap between the absorber and glass cover, the Nusselt number due to natural convection is obtained by the following expressions given by Hollands et al.:

$$Nu = 1 + 1.44\left(1 - \frac{1708\,(\sin 1.8\beta)^{1.6}}{Ra\cos\beta}\right)^{+}\left(1 - \frac{1708}{Ra\cos\beta}\right)^{+} + \left(\frac{Ra\cos\beta}{5830}^{1/3} - 1\right) \quad (3.2)$$

where Ra is the Rayleigh number, β is the tilt angle of the collector, and the + exponent means that the term in the brackets is used if the term is positive.

Absorber

An energy balance is also applied at the absorber where the incident radiation hitting the glass and the effect of the glass transmissivity is balanced by the losses of convection in the air gap between the absorber and the glass cover, the radiation between the absorber and glass cover, and conduction through the tube wall. The energy is then transferred to the working fluid:

$$q_{absorbed} = q_{conv,abs-air} + q_{rad,abs-g} + q_{fluid} \text{ or}$$

with the heat fluxes defined respectively as,

$$\left(\frac{\alpha_{abs}\tau_g}{1-(1-\alpha_{abs})}\right)_g G = h_{air}(T_{abs} - T_{air}) + \varepsilon_{abs}\sigma(T_{abs}^4 - T_g^4) + \left(\frac{T_{abs} - T_{fluid}}{R_{mc}L_{tube}a}\right) \quad (3.3)$$

T_{fluid} is the temperature of the working fluid, L_{tube} is the length of the minichannel tubes, and a is the minichannel tube width. R_{mc} is the total resistance at the minichannel tubes between the absorber and the working fluid as shown in Figure D-2. R_{mc} is also written out as,

$$R_{mc} = R_{abs} + R_{wall} + R_{fluid} = \left(\frac{t_{abs}}{k_{abs}(L_{tube}a)}\right) + \left(\frac{t_{wall}}{k_{wall}(L_{tube}a)}\right) + \left(\frac{1}{\eta_o h_{fluid} A_{tube}}\right) \quad (3.4)$$

where t_{abs} is the thickness of the absorber selective coating, k_{abs} is the thermal conductivity of the absorber selective coating, t_{wall} is the thickness of the minichannel tube wall, k_{wall} is the thermal conductivity of the material of minichannel tubes, and A_{tube} is the total surface area of one minichannel tube. t_{wall} and k_{wall} will depend on whether aluminum (t_{Al} and k_{Al}) or copper

(t_{Cu} and k_{Cu}) minichannel tube collector is considered. h_{fluid} is the single-phase heat transfer coefficient of the working fluid and is given as,

$$h_{fluid} = \frac{k_l Nu_{UD}}{D_h} \tag{3.5}$$

Figure D-2: Resistances at the Absorber

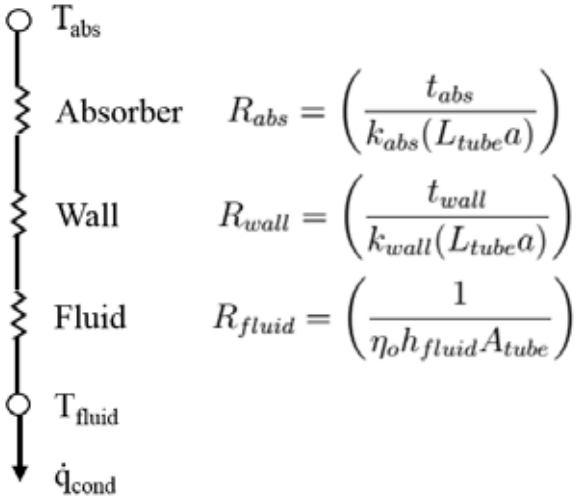

where k_l is the thermal conductivity of the fluid, D_h is the hydraulic diameter and Nu_{UD} is the Nusselt number depending on the dimensions of the minichannel tube and based on Incropera et al. [28]. η_o is the overall fin efficiency and is calculated by,

$$\eta_o = 1 - \frac{N_{fin} A_{fin}}{A_{tube}} (1 - \eta_{fin}) \tag{3.6}$$

The efficiency of the fin, η_{fin} is described as

$$\eta_{fin} = \frac{\tanh(mL_{fin})}{mL_{fin}} \quad (3.7)$$

where $m = \sqrt{\frac{2h_{fluid}(t_{web}+L_{tube})}{k_{wall}t_{web}L_{tube}}}$, N_{fin}

is the number of fins in one minichannel tube, A_{fin} is the surface area of one fin, L_{fin} is the fin length, and t_{web} is the web thickness.

Working Fluid

The heat flux transferred to the working fluid can be expressed by:

$$q_{fluid} = \frac{\dot{m}C_p\Delta T}{L_{tube}W_{major}} \quad (3.8)$$

where $\dot{m}$ is the mass flow rate of the working fluid, C_p is the specific heat of the working fluid, ΔT is the difference of the outlet and inlet temperature $\Delta T = T_{out} - T_{in}$, and W_{major} is the major or width of one minichannel tube.

Model Validation

By using Engineering Equation Solver (EES), the mathematical model was solved using the Newton-Raphson iterative scheme to solve the system of nonlinear equations [30]. The mathematical model allowed us to simulate the performance of the minichannel solar collector for aluminum and copper configurations. For model validations, the experimental data was compared to the results obtained with the experimental set-up. Five input variables are required to run the simulations that were taken directly from the experimental data: inlet temperature T_{in}, solar irradiance G_S, volumetric flow rate V, ambient temperature T_∞, and ambient air velocity v. Figure 3.3 shows the model validation comparing the thermal efficiency between the experimental test data and numerical mathematical model of the aluminum minichannel solar collector for Spring operating conditions. The efficiency is plotted against a common parameter used in solar energy research, $(T_{inlet} - T_\infty)/G_S$. Figure D-3 shows good agreement is obtained between the experiment data and simulation results. Figure D-4 shows the same Spring operating conditions for model validation except the efficiency is plotted against the time of day. The mathematical model is steady-state and this can be seen in the figure. The

mathematical model does not capture the transient and thermal inertia effects seen at the beginning and at the end of the day.

The model can be used to analyze the effect the material used for the minichannel tubes, for example, aluminum or copper. When aluminum properties were used for the minichannel tube, results of the model show that the last term of Equation 3.4 (reproduced below) which represents the overall thermal resistance to the working fluid is two orders of magnitude larger than the other two thermal resistances in that equation:

$$R_{mc} = R_{abs} + R_{wall} + R_{fluid} = \left(\frac{t_{abs}}{k_{abs}(L_{tube}a}\right) + \left(\frac{t_{wall}}{k_{wall}(L_{tube}a}\right) + \left(\frac{1}{\eta_o h_{fluid} A_{tube}}\right) \quad (3.4)$$

Figure D-3: Thermal Efficiency Comparison

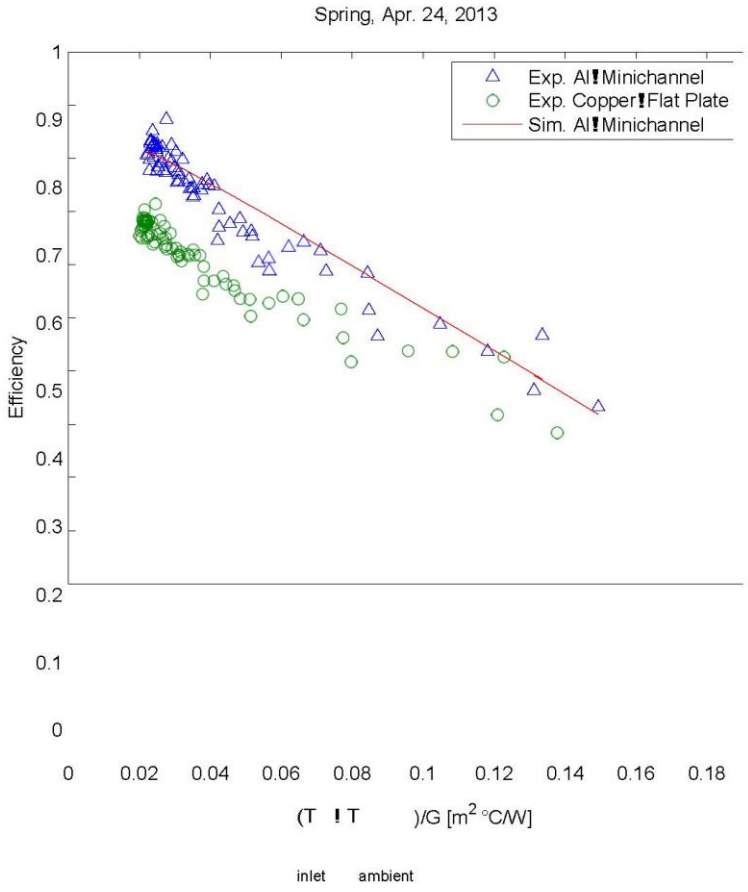

Thermal efficiency comparison of experimental aluminum minichannel and copper flat-plate solar collectors, and mathematical model of aluminum minichannel solar collector in terms of $(T_{inlet} - T_{\infty})/G_S$ in Spring, April 24, 2013.

Figure D-4: Thermal Efficiency Comparison

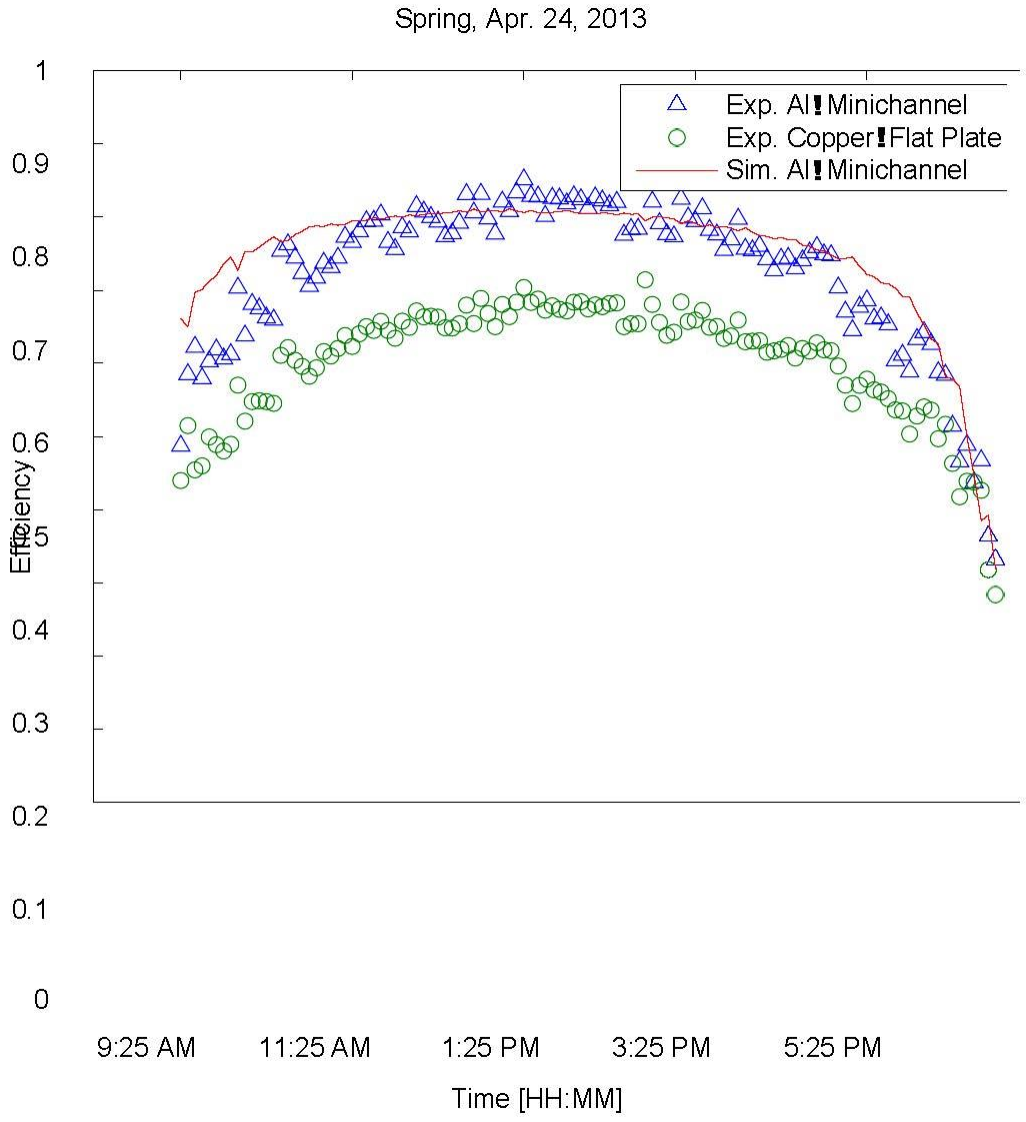

Thermal efficiency comparison of experimental aluminum minichannel and copper flat-plate solar collectors, and mathematical model of aluminium minichannel solar collector in terms of time of day in Spring, April 24, 2013.

Furthermore, the resistance due to convection does not depend on the minichannel tube material. Therefore if operating within the typical temperature range of solar water heaters, there is no major loss of performance when using aluminum as the material for the minichannel tube instead of copper. In addition, the lower cost of aluminum in comparison to copper makes aluminum minichannel solar water heater an attractive alternative to the more conventional copper flat-plate solar water heater designs. More information about cost analysis of the aluminum minichannnel is discussed in Chapter 6. Due to the loss of mechanical properties when aluminum is exposed to higher temperatures, copper or other materials is recommended as minichannel tube material for solar collector designs operating at a medium to high temperatures.

Aluminum Minichannel Solar Water Heater Performance under Year-Round Weather Conditions

See attached article “Aluminum minichannel solar water heater performance under year-round weather conditions (Azucena Robles, Van Duong, Adam J. Martin, Jose L. Guadarrama, Gerardo Diaz, Journal of Solar Energy, Issue 110, 2014 p. 356-364).

Available online at www.sciencedirect.com

ScienceDirect

Solar Energy 110 (2014) 356 364

SOLAR ENERGY

www.elsevier.com/locate/solener

Aluminum minichannel solar water heater performance under year-round weather conditions

Azucena Robles, Van Duong, Adam J. Martin, Jose L. Guadarrama, Gerardo Diaz *

School of Engineering, University of California-Merced, 5200 North Lake Rd., Merced, CA 95343, USA

Received 25 March 2014; received in revised form 6 July 2014; accepted 21 September 2014

Communicated by: Associate Editor Ursula Eicker

Abstract

In the United States, water heaters are the second highest source of energy usage in households. A wide variety of water heater configurations are available in the market, some of which have higher operating costs than other configurations. Although the most common systems utilize natural gas or electricity to heat water, the use of solar water heaters is becoming more widespread mainly due to the low operating costs associated with this technology. Common designs of solar water heaters include flat-plate collectors and evacuated tubes with a heatpipe attached to an absorber fin. In general, copper is used for the fabrication of these collectors due to its excellent heat transfer properties. However, other thermal designs allow the use of alternative materials without loss of performance. This paper discusses the performance of an aluminum-based minichannel solar water heater under several weather conditions throughout a year.

Keywords: Minichannel; Solar collector; Aluminum

1. Introduction

Water heating accounts for a significant amount of energy consumption in the residential and commercial sectors. For instance, residential water heating is often the second largest energy use in a house and, in many cases, it accounts for nearly a quarter of the overall household energy consumption. According to Maguire (2012), there are many different water heater models available in the market, however, the most common water heaters use electricity or natural gas, with 40% of U.S. homes using electric water heaters and 53% using natural gas; the remaining homes use other fuel sources such as fuel oil, propane, wood, or solar. Standard electrical resistance storage tanks have been found to have the highest energy cost compared to other technologies (NewportPartners, 2011). Other common configurations have lower operating costs but require the use of natural gas, propane, or other fuels.

The use of solar energy as a mean of heating water has been a topic of interest since 1891 when Clarence Kemp patented the Climax solar water heater which became the first commercial model (Kemp, 1891). In general, solar thermal systems, such as solar water heaters, provide the capability of generating low to medium grade heat in a sustainable way and for a variety of applications due to the relatively large range of operating temperatures that different collector configurations provide. With the ongoing improvements in efficiency, solar thermal applications are increasingly being adopted in many areas of the world. The different configurations available include non-concentrating collectors for low-temperature applications and concentrating collectors for medium-temperature applications which may or may not require tracking. Tian and Zhao (2013)

* Corresponding author. Tel.: +1 209 228 7858.
E-mail address: gdiaz@ucmerced.edu (G. Diaz).

http://dx.doi.org/10.1016/j.solener.2014.09.031
0038-092X/

Nomenclature

a	width of one aluminum tube (m)
A	area (m^2)
C_p	specific heat of glycol–water mixture ($kJ\ kg^{-1}\ K^{-1}$)
D	diameter (m)
G_s	total incident radiation (W/m^2)
h	heat transfer coefficient (W/m^2-K)
k	thermal conductivity (W/m-K)
L	length (m)
$\dot{m}$	mass flow rate ($kg\ s^{-1}$)
N_f	number of fins in an aluminum tube
Nu	Nusselt number
$\dot{Q}$	heat transfer rate (W)
R	thermal resistance (K/W)
Ra	Rayleigh number
t	thickness (m)
T	temperature (K)
TIG	tungsten inert gas
U_L	overall heat transfer coefficient at the absorber surface
v	velocity of the ambient air surrounding the collector (m/s)
W_t	tube spacing

Subscripts

Abs	absorber
Al	aluminum
air	air between glass cover and absorber
c	collector
e	external
f	fin of the minichannel tube
fluid	working fluid
fp	flat plate collector
g	glass cover
i	internal
in	inlet
mc	minichannel collector
out	outlet
sky	sky
t	tube
web	web of the aluminum tube
wall	tube wall
∞	ambient

Greek symbols

α	absorption coefficient
β	tilt angle
ϵ	emissivity
η	fin efficiency
ρ	reflectivity
σ	Stefan–Boltzmann constant (W/m^2-K^4)
τ	transmissivity

provide a recent review of solar collectors and thermal energy storage applications.

Since Kemp's Climax solar water heater, a number of collector designs have been proposed which include flat plate (Duffie and Beckman, 2006), evacuated tube collectors (Ayompe and Duffy, 2013), and units requiring compound parabolic concentrators (Rabl et al., 1980). In general, solar water systems are classified as "passive", i.e. do not require any source of power, or "active", meaning that they require some form of input power to operate. Solar water heaters can also be characterized as (a) open systems where water flows directly through the collectors, or (b) closed systems where a working fluid flows through the collectors and exchanges energy with water inside a storage tank by means of a heat exchanger. A review of the most recent advances in solar water heating systems can be found in Shukla et al. (2013).

A key issue that remains a subject of intense research relates to effectively transferring the energy obtained from the sun to the working fluid. Increasing the efficiency of solar water heaters has the potential to have a high impact on the consumption of natural gas and other fuels in the residential and commercial sector. Currently, two configurations of solar water heaters capture most of the residential market: (a) flat-plate solar collectors and (b) evacuated-tube solar collectors. In a flat-plate design, a round-pipe is attached to a thin absorber plate usually by ultrasonic welding. Only a small section of the pipe's circumference has good contact with the absorber through the weld. The pipes are equally spaced along the width of the water heater and water flows in parallel flow. Some designs use a serpentine coil attached to the absorber plate but this configuration increases pressure drop significantly. Jafarkazemi and Ahmadifard (2013) concluded that the performance of this solar collector configuration is highly dependent on changes made to its design parameters.

The second common configuration is the evacuated-tube solar collector design, usually consisting of a heat-pipe welded to an absorber fin. The working fluid is moved by thermosyphon effect and the energy absorbed by the heat pipe is transferred to the condensing section of the heat pipe that is in contact with the water inside the tank. Some of the main issues with this design are: the relative small size of the condenser section, which limits the rate of heat transfer absorbed by the heat pipe (Liang et al., 2011), and maintaining vacuum conditions over time (Ma et al., 2010).

Diaz proposed the use of minichannel tubes in solar collectors as a means of improving heat transfer to the

working fluid (Diaz, 2008; Sharma et al., 2011a). The performance of an evacuated-tube minichannel solar collector was analyzed numerically showing increased thermal efficiency compared to experimental data from an evacuated tube solar collector without minichannels (Sharma and Diaz, 2011b). Very recently Mansour (2013) tested a 0.6 m^2 copper minichannel solar flat-plate collector and developed a mathematical model to study its performance. He found a heat removal factor that was 16.1% higher for the minichannel-based collector compared to a conventional flat-plate configuration.

Minichannel heat exchangers, sometimes called microchannels, have been successfully utilized in the automotive, air conditioning, and electronics cooling industry due to their improved performance and compact size compared to round-tube plate-fin heat exchangers (Steinke and Kandlikar, 2004; Yun et al., 2007; Kim and Han, 2008), but they are gradually being introduced to the solar thermal industry. A few companies such as Chengyi and Savo Solar are currently manufacturing flat solar water heaters with minichannel tubes. However, long term performance data of these types of collectors is not currently available in the literature. This paper describes the design, manufacturing, testing and numerical simulation of a non-evacuated aluminum-based minichannel solar water heater tested under year-round weather conditions.

2. Minichannel solar water heater design

Aluminum minichannel tubes are usually produced by extrusion. They have a nearly rectangular cross sectional area with either square or circular ports inside. The availability of extruded aluminum tubes, a 100 mm × 2 mm MPE (multi-port extrusions) tube profile from Hydro was selected to manufacture the minichannel solar water heater. The tubes were inserted inside parallel slots machined on an aluminum header with an internal diameter of 25.4 mm, as shown in Fig. 1. Black Chrome (EC Series) selective coating with a maximum absorptivity and emissivity of 95% and 12%, respectively, was sprayed on the outer surface of the minichannel tube avoiding the need for an absorber fin. This provides a significant advantage for solar collectors since the working fluid is directly in contact with the tube wall that receives solar irradiation, thus, reducing the overall thermal resistance, as depicted in Fig. 2.

The minichannel solar water heater was constructed as a prototype to study preliminary performance and manufacturing methods, thus, the spacing between the tubes was not optimized for mass manufacturing of this design. The spacing between tubes was determined by the size of the TIG welding nozzle used to attach the tubes to the header. A picture of the collector before applying the selective coating is shown in Fig. 3. The aluminum water heater was inserted inside a commercially available metallic frame with a width of 1220 mm and a length of 3050 mm that was covered with an extra clear patterned glass from Solite which has a transmissivity of 0.909.

2.1. Hot water storage system

A closed loop configuration was utilized with a mixture of 50% propylene glycol and 50% water by volume. The propylene glycol mixture exchanges energy with water inside the storage tank by means of an internal coil heat exchanger. A standard commercially available 80-gallon (302.8 liters) water storage tank from SunEarth Inc. was used in the installation depicted in the schematic drawing of the experimental setup shown in Fig. 4. Although the thermophysical properties of the glycol mixture are inferior to water, the mixture allows operation of the system at below-freezing ambient conditions minimizing the chances of bursting tubes due to ice formation inside the tube ports. A 1/4 HP Grundfos pump was used to move the working fluid around the closed loop system.

Data were collected with a National Instruments CompactDAQ system connected to LabVIEW which recorded

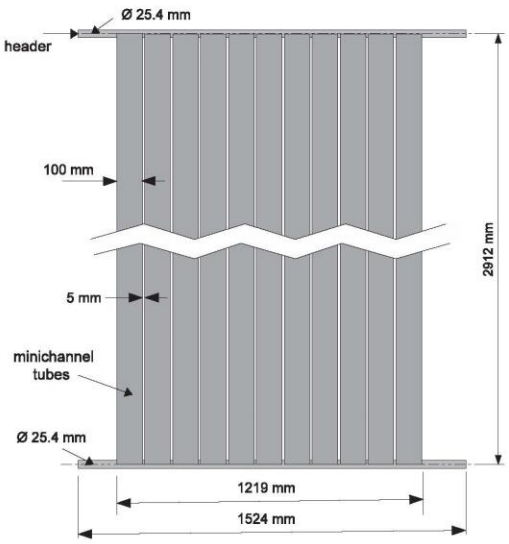

Fig. 1. Dimensions of the minichannel collector.

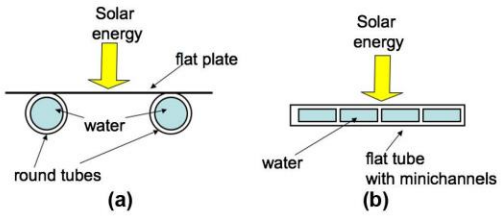

Fig. 2. Heat transfer in flat plate and minichannel solar water heater.

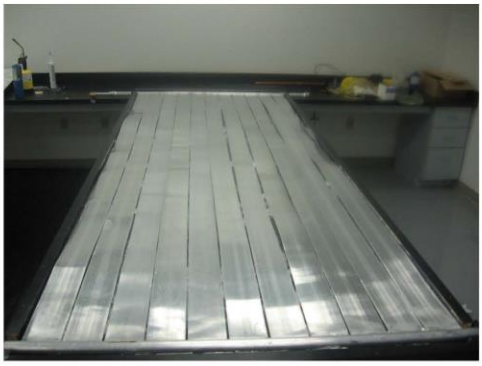

Fig. 3. Minichannel tube solar water heater before application of selective coating.

inlet and outlet temperatures at the collector, as well as, water temperature inside the storage tank. Type K thermocouples with a range between −200 °C to 1250 °C from Omega were utilized which have a standard limit of error of 1.1 °C over the entire scale. The volume flow rate through the water heater was measured with a Grundfos low-flow sensor Model # VFS 1-20 with an accuracy of ±1.5 % of the full scale, and the solar irradiation was measured with a Precision Spectral Pyranometer (PSP) from Eppley installed on the same plane as the collector. The solar water heater was installed on the roof of the laboratory building at the University of California at Merced (+37°22′28.59″, −120°34′38.10″) which has an angle of 18° with respect to the ground. The flow through the collector between inlet and outlet was oriented North-to-South.

The system was controlled directly from LabVIEW with the close loop pump being turned on when the PSP signal was greater than 150 W m^{-2}. The discharge valve from the storage tank was automatically controlled to open whenever the temperature inside the tank reached 55 °C allowing cold water from the water supply to flow into the water tank, lowering its temperature. The discharge valve remained open until the temperature inside the tank fell below 30 °C. At this point, the discharge valve was closed and the water temperature inside the storage tank was allowed to rise again due to the exchange of energy with the glycol mixture flowing through closed loop. The system has been operational since February 2013 with data being recorded for every minute during daily operation.

2.1.1. Conventional flat-plate configuration

In order to compare the performance of the new minichannel-based design with a benchmark configuration, a conventional copper round-tube flat-plate solar water heater with similar dimensions as the aluminum collector was constructed and installed adjacent to the aluminum minichannel solar water heater. The round-tube flat-plate collector was built with equivalent ratio of free flow area to absorber area as found in commercial designs. Components such as storage tank, pump, piping, and sensors were replicated in a closed loop system operating under the same conditions as the closed loop system for the minichannel collector. Both water heater systems operated independently

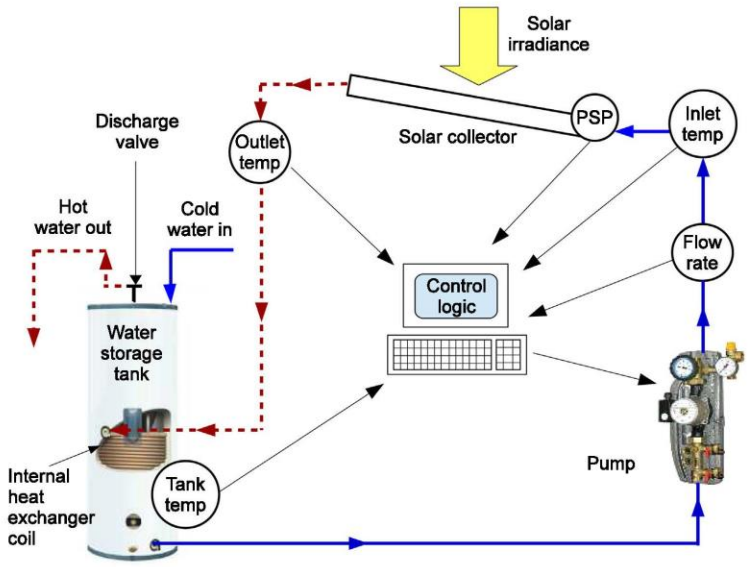

Fig. 4. Schematic of experimental set-up.

Table 1
Characteristic properties of aluminum minichannel and copper flat plate solar water heaters.

Parameter	Minichannel collector	Flat-plate collector	Units
Frame length	3048	3048	mm
Frame width	1219	1219	mm
Number of tubes	11	10	
Absorber area	3.20	3.61	m^2
Absorber fin thickness		0.2032	mm
Glass transmissivity	0.909	0.909	
Total free flow area	1015.5	712.2	mm^2
Hydraulic diameter (each tube)	1.42	9.53	mm
Ratio of free flow area to absorber area	317.3	197.3	mm^2/m^2
Collector mass (including headers and without frame)	11.48	15.22	kg
Thermal inertia $\left(\sqrt{k\rho c_p}\right)$	22,492.7	34,438.3	$J\,m^{-2}\,K^{-1}\,s^{-1/2}$

from each other. Table 1 shows some of the characteristic dimensions of the two solar collectors.

3. Results and discussion

This section discusses the experimental performance of the aluminum minichannel and conventional flat-plate solar water heaters operating under a variety of ambient conditions between February 2013 to February 2014.

3.1. Performance of aluminum minichannel collector

Fig. 5(a) shows measured data of the inlet temperature to the solar water heater (solid green line), outlet temperature (dotted red line), and storage tank temperature (dashed blue line) for typical conditions during Spring with ambient temperatures fluctuating between 16 °C and 28 °C. The measured volumetric flow rate through the collector corresponded to 6.4 liters per minute. Under these conditions, an increase of approximately 23 °C in the tank temperature is observed over the nearly 9 h of operation during the day. The maximum outlet temperature at the collector reached 58.1 °C and the maximum difference between inlet an outlet temperatures at the collector was 4.6 °C at 2:14 pm. Solar irradiance, shown on the right vertical axis, reached a maximum value of 822 W/m^2 but exhibited variability due to cloud coverage during the afternoon. The maximum heat transfer rate obtained was 1.84 kW and the energy per unit of area for the entire day of operation was 3.2 kWh/m^2.

Fig. 5(b) shows the performance of the aluminum minichannel solar water heater on a summer day with ambient temperatures between 21 °C and 33 °C. The maximum temperature difference between inlet and outlet reached 4.9 °C at 2:05 pm and the maximum outlet temperature (dotted red line) reached 63.3 °C. It is observed that the storage tank temperature started at 31.6 °C in the morning and reached 55.1 °C at 5:27 pm triggering the controller to open the discharge valve, since the maximum water temperature in the tank was limited to 55 °C. At 5:48 pm the discharge valve was closed and the temperature of the water inside the tank started to rise again. The solar irradiance reached a maximum of 867 W/m^2 at 2:24 pm.

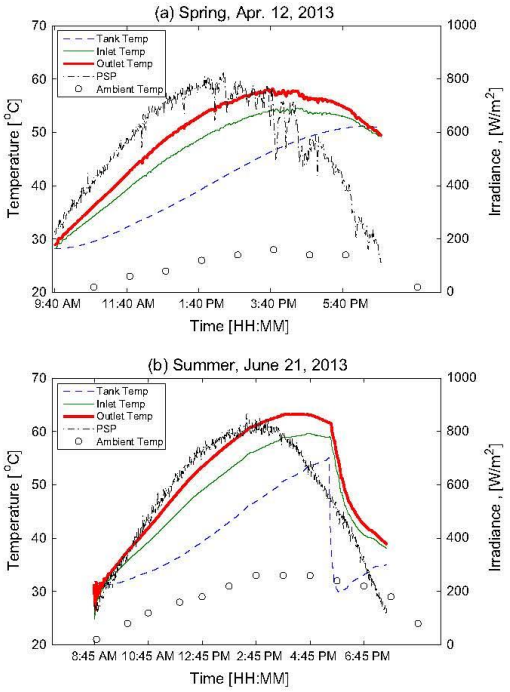

Fig. 5. Performance of aluminum minichannel solar water heater. (a) Spring, (b) Summer.

3.2. Comparison with conventional flat plate configuration

Fig. 6(a–d) show the comparison of the temperature measured at each storage tank for the minichannel and conventional flat-plate collectors for operating conditions covering the entire year. Fig. 6(a) corresponds to winter conditions where ambient temperatures fluctuated between

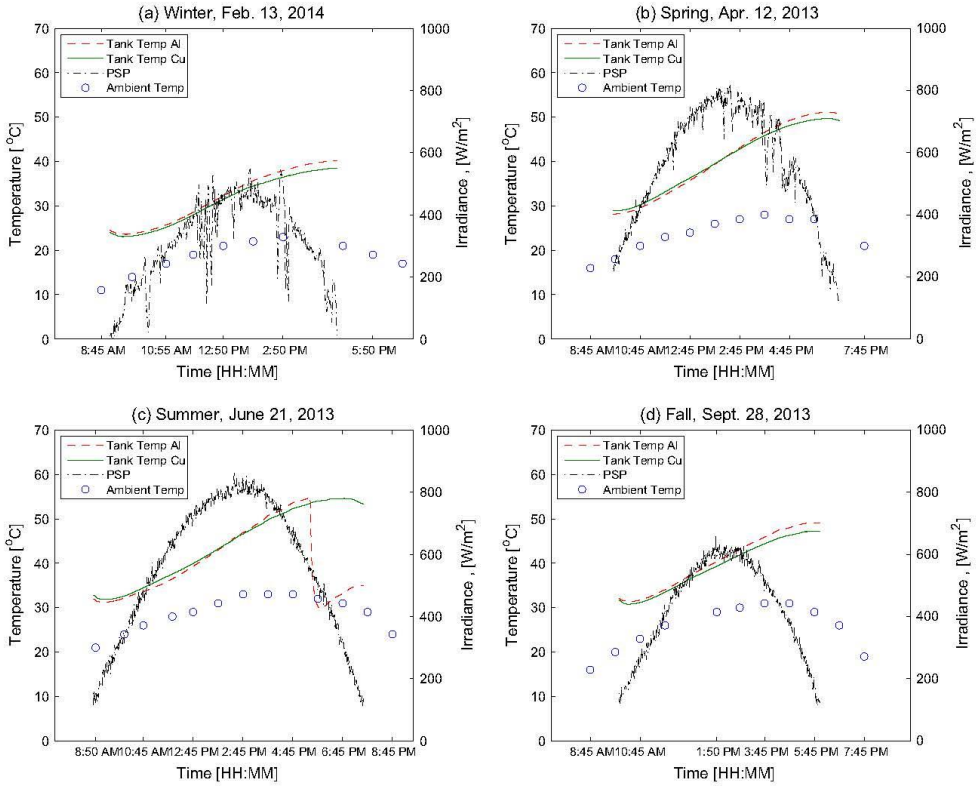

Fig. 6. Comparison of storage tank temperature. (a) Winter, (b) Spring, (c) Summer, (d) Fall.

11 °C and 23 °C during the seven and a half hours of operation during the day where the maximum solar irradiance reached 547 W/m^2 at 1:42 pm. The water temperature inside the storage tank for the minichannel collector started 0.4 °C above the temperature of the water inside the storage tank for the flat plate collector, which started at 24.3 °C. It is seen that at 4:35 pm the controller shut down the pumps due to the low value of solar irradiance. At that instant, the storage tank for the minichannel collector showed a water temperature of 40.2 °C compared to 38.5 °C of the storage tank for the copper flat-plate collector, indicating a 1.3 °C gain in performance by the minichannel solar water heater compared to the flat-plate collector. The gain in temperature during the day can be observed more clearly in Fig. 6(b) which depicts operating conditions during Spring. The water inside the storage tank for the minichannel collector started at 28.1 °C which is 0.7 °C below the water in the flat-plate collector tank. The systems operated for nine hours raising the water temperature of the storage tank for the minichannel and flat-plate collectors by 22.6 °C and 20.3 °C, respectively. Thus, the minichannel collector generated a net gain in water temperature at the storage tank of 2.23 °C with respect to the conventional collector design. This difference is significant considering the large volume of nearly 300 liters of water inside each storage tank. Fig. 6(c) shows the performance comparison for a summer day. The storage tank for the minichannel collector started at a temperature of 29.9 °C, which was 0.9 degrees below the temperature of the storage tank for the conventional flat plate collector. It is observed that the discharge valve of the storage tank for the minichannel collector was opened at 5:37 pm since the temperature of the water reached the safety limit of 55 °C. On the other hand, the temperature of the water inside the storage tank for the flat-plate collector did not reach the safety limit so the tank was not discharged during the day. Flow rates for both collectors corresponded to 6.57 liters/min for the minichannel collector and 6.16 liters/min for the flat-plate collector with both pumps set at high speed. The maximum heat transfer rate was 1.92 kW and 1.77 kW for the minichannel and flat plate collector, respectively, and the energy per unit area collected during eleven hours of operation during the day reached 13.4 kWh/day for the minichannel collector and 12.1 kWh/day for the flat plate collector. It is observed that, in general, during summer conditions both storage

tanks reached the maximum operational temperature limit during the day which triggered the opening of the discharge valve. However, the water inside the tank for the minichannel collector consistently reached the safety limit approximately an hour earlier than the water in the tank for the conventional flat-plate collector. Finally, under Fall weather conditions with low solar irradiance and ambient temperatures, the water inside the tank did not reach the safety limit for any of the collectors, so the discharge valves were not open, as shown in Fig. 6(d). Nonetheless, the minichannel collector consistently showed improved performance with respect to the conventional collector design. For case (d) in Fig. 6, the water in the tank gained 17.0 °C for the minichannel collector and 15.6 °C for the flat-plate collector during 8 h of operation.

The thermal efficiency obtained with each collector was determined by taking the ratio between the heat transfer rate at the collector divided by the solar energy reaching the absorber:

$$\eta = \frac{\dot{Q}_c}{\left(\frac{\alpha_{Abs}\tau_g}{1-(1-\alpha_{Abs})\rho_g}\right) G_s A_{Abs}} \tag{1}$$

where $\dot{Q}_c = \dot{m}C_p(T_{out} - T_{in})$, $\dot{m}$ is the mass flow rate of glycol mixture flowing through the collector, C_p is the specific heat of the glycol solution, G_s is the total incident radiation per unit of area, A_{Abs} is the absorber area, and T_{out} and T_{in} are the outlet and inlet temperatures at the collector, respectively. It is observed that the absorber areas of the collectors are different with the minichannel collector area being $A = NWL$, where $N = 11$ corresponds to the number of minichannel tubes used to build the solar water heater, $W = 0.1$ m is the width of each minichannel tube, and $L = 2.92$ m is the length of the minichannel tubes. The area of the flat-plate copper collector corresponded to the area of the plate inside the collector metallic frame. A summary of the absorber areas is found in Table 1.

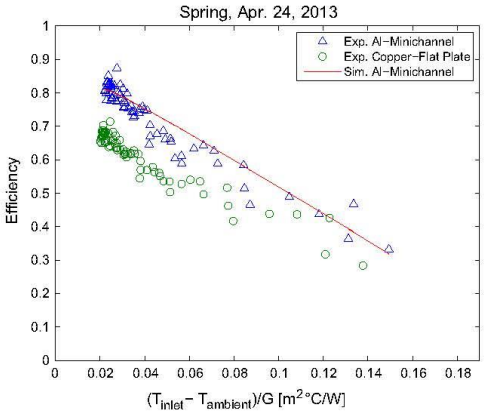

Fig. 7. Comparison between solar collector experimental thermal efficiency and mathematical model in terms of $(T_{inlet} - T_{ambient})/G)$.

Fig. 7 shows the comparison of the thermal efficiencies obtained experimentally for each collector during Spring operating conditions. The minichannel collector shows an average improvement in thermal efficiency of 12% with respect to the flat-plate collector during the day. The difference can be explained by analyzing the thermal resistances of both collectors. The thermal resistance from fluid to air-gap for the conventional flat plate collector is obtained from Duffie and Beckman (2006):

$$R_{fp} = W_t\left[\frac{1}{U_L[D_e + (W_t - D_e)\eta_{fp}]} + \frac{1}{\pi D_i h_{fp,i}}\right] \tag{2}$$

where U_L is the overall heat transfer coefficient at the absorber surface, W_t is the tube spacing, D_e is the tube external diameter, D_i is the tube internal diameter, $h_{fp,i}$ is the internal heat transfer coefficient, and the fin efficiency is given by

$$\eta_{fp} = \frac{\tanh[m(W_t - D_e)/2]}{m(W_t - D_e)/2} \tag{3}$$

with $m = \sqrt{\frac{U_L}{k_{fp}t_{fp}}}$, where k_{fp} and t_{fp} are the thermal conductivity and fin thickness, respectively. On the other hand, the thermal resistance for the minichannel collector (R_{mc}) is given by Eq. (7) described in the next section. Under the operating conditions shown in the figure, R_{fp} is an order of magnitude larger than R_{mc}, illustrating the beneficial aspects of the minichannel design which reduces the thermal resistance by avoiding the use of a thin sheet absorber attached to a tube. As opposed to flat-plate collectors, where there is a temperature gradient in between tubes at the absorber fin, which can reach a few centigrade degrees, the minichannel tube has a uniform wall temperature across its width.

4. Mathematical model

A mathematical model based on an energy balance of the aluminum-based minichannel solar water heater was developed adapting the heat transfer analysis described in Fonseca (2008) and in Duffie and Beckman (2006). The following assumptions were made: (a) steady-state conditions, (b) uniform surface temperature, (c) all minichannel ports have the same dimensions.

4.1. Glass cover

An energy balance applied at the glass cover, which includes the solar irradiance, radiative exchange between absorber and glass, convection between absorber and glass, and the losses due to convection to the ambient, radiation to the sky, and glass transmissivity, is as follows:

$$G_s + \left(\frac{1}{\frac{1}{\epsilon_g}+\frac{1}{\epsilon_{Abs}}-1}\right)\sigma\left(T_{Abs}{}^4 - T_g^4\right) + h_{air}(T_{air}-T_g) = h_{g,air}(T_g - T_\infty) + \epsilon_g\sigma\left(T_g{}^4 - T_{sky}^4\right) + \left(\frac{\alpha_{Abs}\tau_g}{1-(1-\alpha_{Abs})\rho_g}\right)G_s \quad (4)$$

where G_s is the total incident radiation, T_{Abs} is the temperature at the absorber, T_g is the temperature at the glass, h_{air} is the convection heat transfer coefficient of the air between the glass and absorber, and T_{air} is the temperature of the air between the glass and absorber. $h_{g,air}$ represents the convection heat transfer coefficient between the glass and ambient air given by the empirical expression: $h_{g,air} = 2.8 + 3v$ (Fonseca, 2008; Khoukhi and Maruyama, 2005). The velocity of the ambient air in the equation is represented by v, T_∞ corresponds to the ambient temperature, and T_{sky} is the sky temperature related to the ambient temperature by the equation: $T_{sky} = 0.0552T_\infty^{1.5}$ (Khoukhi and Maruyama, 2005). Finally ϵ_g is the glass emissivity, ϵ_{Abs} is the absorber emissivity, α_{Abs} is the absorptivity of the absorber, τ_g is the transmissivity of the glass, and ρ_g is the glass reflectivity.

4.2. Absorber-cover gap

The Nusselt number due to natural convection between absorber and glass cover is obtained by the expression developed by Hollands et al. (1976):

$$\mathrm{Nu} = 1 + 1.44\left[1 - \frac{1708(\sin 1.8\beta)^{1.6}}{\mathrm{Ra}\ \cos\beta}\right]\left[1 - \frac{1708}{\mathrm{Ra}\ \cos\beta}\right]^+ + \left[\left(\frac{\mathrm{Ra}\ \cos\beta}{5830}\right)^{1/3} - 1\right]^+ \quad (5)$$

where Ra corresponds to the Rayleigh number, β is the tilt angle, and the + exponent indicates that the term in brackets is considered only if it is positive.

4.3. Absorber

Applying an energy balance at the absorber yields the following expression:

$$\left(\frac{\alpha_{Abs}\tau_g}{1-(1-\alpha_{Abs})\rho_g}\right)G_s = h_{air}(T_{Abs}-T_{air}) + \epsilon_{Abs}\sigma\left(T_{Abs}{}^4 - T_g^4\right) + \left(\frac{T_{Abs}-T_{fluid}}{R_{mc}L_t a}\right) \quad (6)$$

where the incident radiation due to the glass transmissivity is balanced by the losses due to convection to the air gap between the absorber and the glass, radiation between absorber and glass, and the energy rejected to the working fluid, and where T_{fluid} is the temperature of the fluid, R_{mc} is the total thermal resistance between absorber and working fluid, L_t is tube length, and a is tube width.

The total thermal resistance is obtained from Eq. (7),

$$R_{mc} = \left(\frac{t_{Abs}}{k_{Abs}(L_t a)}\right) + \left(\frac{t_{wall}}{k_{Al}(L_t a)}\right) + \frac{1}{\eta_o h_{fluid} A_t} \quad (7)$$

where t_{Abs} is the thickness of the absorber selective coating, k_{Abs} is the thermal conductivity of the absorber, t_{wall} is the thickness of the tube wall, k_{Al} is the thermal conductivity of aluminum, η_o is the overall fin efficiency, h_{fluid} is the heat transfer coefficient of the fluid, and A_t is the total surface area of one aluminum tube. The overall fin efficiency is calculated as follows:

$$\eta_o = 1 - \frac{N_f A_f}{A_t}(1-\eta_f) \quad (8)$$

$$\eta_f = \frac{\tanh(mL_f)}{mL_f} \quad (9)$$

where $m = \sqrt{\frac{2h_{fluid}(t_{web}+L_t)}{k_{Al}t_{web}L_t}}$, t_{web} is the web thickness, N_f is the number of fins in an aluminum tube, A_f is the surface area of the fin and L_f is the fin length.

4.4. Model validation

Engineering Equation Solver (EES, 2014) was used to solve the mathematical model using a Newton–Raphson iterative scheme to solve the system of nonlinear equations. The experimental data was compared to the results obtained with the model. Five input variables are required to run the simulations which were obtained directly from the experimental data, i.e. inlet temperature, T_{in}, solar irradiance, G_s, volumetric flow rate, $\dot{V}$, ambient temperature, T_∞, and ambient air velocity, v. Fig. 7 shows the comparison of thermal efficiency between test data and the numerical model for Spring operating conditions. Efficiency is plotted against $(T_{inlet} - T_{ambient})/G$, where good agreement is obtained between experiments and simulations.

The model is used to analyze the effect of the material used for the minichannel tubes, i.e. aluminum or copper. Using aluminum properties for the tube material, the results of the model show that the last term in Eq. (7) which corresponds to the convective resistance to the working fluid is two orders of magnitude larger than the other two thermal resistances. In addition, the resistance due to convection does not depend on the tube material. Thus, within the operating range of temperatures typical of solar water heaters, there is no major loss of performance when using aluminum instead of copper in minichannel tubes. Also, the lower cost of aluminum with respect to copper makes aluminum minichannel solar water heaters an attractive alternative to the more conventional flat-plate designs. However, due to the loss of mechanical properties of aluminum at higher temperatures, copper or other materials would be required as tube materials for collector designs operating at medium to high temperatures.

5. Conclusion

Experimental results of an aluminum based minichannel solar water heater currently being tested at the University

of California at Merced are presented. The design utilizes minichannel tubes attached to headers and does not require a flat fin attached to the tube to transfer heat to the working fluid. The performance of the minichannel collector is compared against a conventional copper flat-plate collector utilizing the same external components and operating conditions for both independent systems. Improved efficiency of the aluminum based minichannel solar water heater was due to an improved thermal design. Results show an average increase in thermal efficiency of 13% obtained with the minichannel collector, as well as, higher energy collection during the day. A mathematical model of the minichannel collector is developed and validated with the experimental data obtained during the operation of the system throughout the year. The model shows that the lower thermal conductivity of aluminum does not translate into a loss of performance of these collectors. However, minichannel tubes manufactured in copper or similar materials would be needed for operation at medium-to-high temperatures.

Acknowledgments

This project is being funded by the California Energy Commission Contract # POEF01-M04. The authors also thank Justin McConnell for fabricating the aluminum minichannel collector, and Kevin Rico and Kevin Balkoski for their help with the system installation.

References

Ayompe, L.M., Duffy, A., 2013. Thermal performance analysis of a solar water heating system with heat pipe evacuated tube collector using data from a field trial. Sol. Energy 90, 17 28.

Diaz, G., 2008. Performance analysis and design optimization of a minichannel evacuated-tube solar collector. In: Proceedings of ASME IMECE 2008, Paper # IMECE2008-67858. Boston, MA, pp. 1 7.

Duffie, J.A., Beckman, W.A., 2006. Solar Engineering of Thermal Processes. John Wiley & Sons Inc.

EES, 2014. Engineering Equation Solver. F-Chart Software. <http://www.fchart.com/ees/>.

Fonseca, A.T., 2008. Performance assessment of three concentrating solar thermal units designed with xcpc reflectors and evacuated tubes, using an analytical thermal model. Master's thesis, University of California, Merced.

Hollands, K.G.T., Unny, T.E., Raithby, G.D., Konicek, L., 1976. Free convection heat transfer across inclined air layers. Trans. ASME J. Heat Transfer, 98.

Jafarkazemi, F., Ahmadifard, E., 2013. Energetic and exergetic evaluation of flat plate solar collectors. Renew. Energy 56, 55 63.

Kemp, C.M., 1891. Apparatus for utilizing the suns rays for heating water, US patent 451384.

Khoukhi, M., Maruyama, S., 2005. Theoretical approach of a flat plate solar collector with clear and low-iron glass covers taking into account the spectral absorption and emission within glass covers layer. Renew. Energy 30, 1177 1194.

Kim, N.-H., Han, S.-P., 2008. Distribution of air water annular flow in a header of a parallel flow heat exchanger. Int. J. Heat Mass Transfer 51, 977 992.

Liang, R., Ma, L., Zhang, J., Zhao, D., 2011. Theoretical and experimental investigation of the filled-type evacuated tube solar collector with u tube. Sol. Energy 85, 1735 1744.

Ma, L., Lu, Z., Zhang, J., Liang, R., 2010. Thermal performance analysis of the glass evacuated tube solar collector with u-tube. Build. Environ. 45, 1959 1967.

Maguire, J.B., 2012. A parametric analysis of residential water heaters. Master's thesis, University of Colorado.

Mansour, M.K., 2013. Thermal analysis of novel minichannel-based solar flat-plate collector. Energy 60, 333 343.

NewportPartners, 2011. Comparing Residential Water Heaters for Energy Use, Economics and Emissions. Tech. rep., Propane Education and Research Council, Davidsonville, MD.

Rabl, A., O'Gallager, J., Winston, R., 1980. Design and test of non-evacuated solar collectors with compound parabolic concentrators. Sol. Energy 25, 335 351.

Sharma, N., Diaz, G., August 2011a. Minichannel tube solar collector, US patent US 2011/0186043 A1.

Sharma, N., Diaz, G., 2011b. Performance model of a novel evacuated tube solar collector based on minichannels. Sol. Energy 85, 881 890.

Shukla, R., Sumanthy, K., Erickson, P., Gong, J., 2013. Recent advances in the solar water heating systems: a review. Renew. Sustain. Energy Rev. 19, 173 190.

Steinke, M.E., Kandlikar, S.G., 2004. Single-phase heat transfer enhancements techniques in microchannel and minichannel flows. In: Proceedings of Microchannels and Minichannels ASME Conference. ASME, pp. 141 148, iCMM2044-2328.

Tian, Y., Zhao, C.Y., 2013. A review of solar collectors and thermal energy storage in solar thermal applications. Appl. Energy 104, 538 553.

Yun, R., Kim, Y., Park, C., 2007. Numerical analysis on a microchannel evaporator designed for CO_2 air conditioning systems. Appl. Therm. Eng. 27, 1320 1326.